

1 **Microphysical features of typhoon and non-typhoon rainfall observed in Taiwan, an island**
2 **in the northwest Pacific.**

3
4 **Jayalakshmi Janapati¹, Balaji Kumar Seela¹, Pay-Liam Lin^{1,2,3*}, Meng-Tze Lee⁴, Everette**
5 **Joseph⁵**

6 ¹Institute of Atmospheric Physics, Department of Atmospheric Sciences, National Central
7 University, Zhongli district, Taoyuan city, Taiwan

8 ²Earthquake-Disaster & Risk Evaluation and Management Center, National Central University,
9 Zhongli district, Taoyuan city, Taiwan.

10 ³Research Center for Hazard Mitigation and Prevention, National Central University, Zhongli
11 district, Taoyuan City, Taiwan

12 ⁴Department of Atmospheric and Oceanic Sciences, McGill University, Montreal, Quebec,
13 Canada

14 ⁵National Center for Atmospheric Research, Boulder, Colorado

15
16
17 ***Correspondence to:**

18 Prof. Pay-Liam Lin

19 Institute of Atmospheric Physics, Department of Atmospheric Sciences

20 National Central University, Zhongli district, Taoyuan City, Taiwan

21 Phone: 03-422-3294 03-422-7151 ext. 65509

22 E-mail: tlam@pblap.atm.ncu.edu.tw

24 **Abstract**

25 Information about the raindrop size distribution (RSD) is vital to comprehend the
26 precipitation microphysics, improve the rainfall estimation algorithms, and appraise the rainfall
27 erosivity. Previous research has revealed that the RSD exhibits diversity with geographical
28 location and weather type, which perpetrates to assess the region and weather-specific RSDs.
29 Based on long-term (2004 to 2016) disdrometer measurements in north Taiwan, this study
30 pursued to demonstrate the RSD aspects of summer seasons that were bifurcated into two
31 weather conditions, namely typhoon (TY) and non-typhoon (NTY) rainfall. The results show a
32 higher concentration of small drops and a lower concentration of big-size drops in TY compared
33 to NTY rainfall, and this behavior persisted even after characterizing the RSDs into different
34 rainfall rate classes. RSDs expressed in gamma parameters show higher mass-weighted mean
35 diameter (D_m) and lower normalized intercept parameter (N_w) values in NTY than TY rainfall.
36 Forbye, sorting of these two weather conditions (TY and NTY rainfall) into stratiform and
37 convective regimes did reveal a large D_m in NTY than the TY rainfall. The RSD empirical
38 relations used in the valuation of rainfall rate ($Z-R$, D_m-R , and N_w-R) and rainfall kinetic energy
39 ($KE-R$, and $KE-D_m$) were enumerated for TY and NTY rainfall, and they exhibited profound
40 diversity between these two weather conditions. Attributions of RSD variability between the TY
41 and NTY rainfall to the thermodynamical and microphysical processes are elucidated with the
42 aid of reanalysis, remote-sensing, and ground-based datasets.

43

44 **Keywords:** typhoons, non-typhoons, disdrometer, rainfall kinetic energy, north Taiwan

45 **1. Introduction**

46 Taiwan, an island in the northwest Pacific, has complex topography with an outspread
47 from south to north, with an average elevation of about 2 km and peaks of ~ 4 km. The East
48 China Sea bounds Taiwan in the north, the Philippine Sea in the east, Luzon Strait in the south,
49 and the South China Sea in the southwest. This island is affected by two monsoon regimes:
50 southwesterly monsoon (May to August) and northeasterly monsoon (September to April), and
51 these two monsoon regimes were further categorized into winter (December to February), spring
52 (March to April), mei-yu (mid-May to mid-June), summer (mid-June to August), typhoon (May
53 to October), and autumn (September to November) seasons (Chen and Chen, 2003). Among the
54 above-mentioned seasons, the summer seasons, exclusively associated with thunderstorms and
55 typhoons, have intense precipitation than other seasons. Despite reports on the rainfall
56 individualities of different seasons and weather systems in Taiwan (Chen et al., 1999;Chen et al.,
57 2007;Chen et al., 2010;Chen and Chen, 2011;Liang et al., 2017;Tu and Chou, 2013), few
58 attempts were made to explicate rain microphysical aspects, exclusively the RSD characteristics.

59 The RSDs aid in diverse fields like meteorology, hydrology and remote sensing, and
60 afford an insight into the precipitation microphysics (Rosenfeld and Ulbrich, 2003).
61 Characterization of RSDs offers the opportunity to design radar rainfall estimation algorithms
62 (Ryzhkov and Zrnić, 1995), improve the cloud modeling parameterization (McFarquhar et al.,
63 2015), assess the rainfall erosivity relations (Janapati et al., 2019), validate the remote sensing
64 instruments (Liao et al., 2014;Nakamura and Iguchi, 2007), and appraise the rain attenuations
65 (Chen et al., 2011). Owing to the aforementioned implications of RSDs, ample literature exists
66 on RSDs for spatial, seasonal (Thompson et al., 2015;Jayalakshmi and Reddy, 2014;Seela et al.,

67 2017;Seela et al., 2018;Krishna et al., 2016;Seela et al., 2016) variations, storm to storm, within
68 the storm (Kumari et al., 2014;Maki et al., 2001;Jung et al., 2012;Bao et al., 2020;Janapati et al.,
69 2017), and different precipitations (Tokay and Short, 1996;Krishna et al., 2016).

70 Investigations on RSDs have been escalating to illuminate the hydrological (Lin and
71 Chen, 2012;Lu et al., 2008;Janapati et al., 2019;Chang et al., 2017) and microphysical
72 characteristics (Chu and Su, 2008;Jung et al., 2012;Seela et al., 2017;Seela et al., 2018;Lee et al.,
73 2019;Janapati et al., 2020) of diverse precipitating clouds in Taiwan. For instance, Chu and Su
74 (2008) reconnoitered the slope-shape relations for seven precipitation events related to four
75 different weather systems in north Taiwan, and they showed that the derived $\mu-\Lambda$ relation was
76 independent of the gamma RSD moment order. Measurements of a squall line in south Taiwan
77 with ground-based radar and disdrometer revealed that the D_m values in the squall line's
78 convective precipitation were higher than the maritime clusters (Jung et al., 2012). Chang et al.
79 (2009) analyzed the RSDs of landfall typhoons in north Taiwan, and they opined that the
80 interaction of typhoons with Taiwan's complex terrain resulted in the RSDs intermediate to
81 maritime and continental clusters. The comparison study of summer seasons' RSDs between
82 Taiwan and Palau Islands by Seela et al. (2017) revealed more large drops in Taiwan than Palau,
83 and they contended that deeply extended convective clouds with more aerosols in Taiwan
84 resulted in the differences between these two Islands. With the aid of long-term disdrometer
85 measurements for summer and winter seasons in north Taiwan, Seela et al. (2018) noticed a
86 profound disparities in RSDs between these two seasons, and they established the attribution of
87 RSDs differences to the microphysical processes concomitant with deep convective clouds in
88 summer and warm clouds in winter. Furthermore, investigations on microphysical features of six
89 seasons (winter, spring, mei-yu, summer, typhoon, and autumn) in north Taiwan divulged the

90 highest mean D_m values in the summer and highest concentration ($\log_{10}N_w$) in the winter (Lee et
91 al., 2019). A recent study on Indian and Pacific Ocean tropical cyclones manifested higher D_m
92 values in Pacific Ocean tropical cyclones than the Indian Ocean tropical cyclones (Janapati et al.,
93 2020).

94 Efforts have been performed to reveal the RSDs characteristics of tropical cyclones and
95 non-tropical cyclones in India, Australia, China, and Japan (Radhakrishna and Narayana Rao,
96 2010;Kumar and Reddy, 2013;Deo and Walsh, 2016;Chen et al., 2019;Chen et al., 2017).
97 Analysis of tropical cyclones and non-tropical cyclones RSDs in Gadanki (Radhakrishna and
98 Narayana Rao, 2010) and Kadapa (Kumar and Reddy, 2013) unveiled a higher concentration of
99 small drops in tropical cyclones than the non-tropical cyclones. In Australia, Deo and Walsh
100 (2016) illustrated the tropical cyclones and non-tropical cyclones RSDs and demonstrated higher
101 D_m values in non-tropical cyclones than tropical cyclones rainfall. From the 2DVD
102 measurements in East china, Chen et al. (2017) appraised the polarimetric radar variables for
103 typhoons, Mei-yu, and squall line precipitations, and they revealed discrete alterations among
104 these weather systems. Over south China, distinct differences in rain integral parameters of
105 typhoons and squall lines were perceived by Zhang et al. (2019), and they concluded that it is
106 essential to adopt precipitation specific rainfall estimators. Examination of typhoons and mei-yu
107 season RSDs in Japan affirmed maritime behavior in typhoons and continental behavior in mei-
108 yu rainfall (Chen et al., 2019).

109 In contempt of investigations on the typhoon and non-typhoon weather conditions'
110 rainfall characteristics (Chen and Chen, 2011;Tu and Chou, 2013), the microphysical features,
111 especially the summer seasons' RSDs (explicitly segregated to typhoon and non-typhoon

112 weather conditions) are yet to be documented for the Taiwan region. On this account, this study
113 sought to address the following objectives: 1. To investigate alike or unlike individualities of
114 RSDs between the typhoon and non-typhoon rainfall, 2. To identify comparable/unrelated
115 features of typhoon and non-typhoon rainfall to the previous studies, 3. quantification of rainfall
116 rate and rainfall kinetic energy relations, 4. To discern conceivable rationale for peculiarities in
117 the RSDs between typhoon and non-typhoon rainfall events. In this context, to address the
118 aforementioned objectives for the typhoons and non-typhoons rainfall, long-term disdrometer,
119 radar, remote-sensing, and re-analysis data sets were used.

120

121 **2. Data sets used**

122 Taiwan geographic map with National Central University (NCU) (24° 58' N, 121° 10' E)
123 site (indicated with a filled green circle), where the Joss–Waldvogel disdrometer (JWD) (Joss
124 and Waldvogel, 1969) measurements were conducted [for the summer season (16 June to -31
125 August) rainy days of the years 2004 to 2016], is shown in Fig.1. The disdrometer measurements
126 in summer seasons were further classified into a typhoon (TY) and non-typhoon (NTY) weather
127 conditions. In identifying the rainfall amounts of typhoons over Taiwan, previous studies
128 adopted different criteria (Tu and Chou, 2013; Chu et al., 2007; Chen et al., 2010). For instance, if
129 a typhoon center was invaded the rectangular grid box of 21°-26° N and 119°-125° E (Chu et al.,
130 2007) or 19.5°-27.5° and 117.5°-124.5° E (Chen et al., 2010) or 18°-29.5° N and 116°-126° E (Tu
131 and Chou, 2013), the corresponding rain in Taiwan was selected as typhoon induced rain. On the
132 other hand, in the current study, precipitation at the NCU disdrometer site was considered as
133 typhoon-induced rain when the typhoon center was ≤ 500 km from the disdrometer (Janapati et

134 al., 2019), and the rest of the rainy days in summer seasons were categorized as NTY rainy days.
135 With this condition, a total number of 59 TY rainy days (hereafter TY days) and 131 NTY rainy
136 days (hereafter NTY days) were recorded by the NCU JWD from 2004 to 2016 (excluding 2008
137 and 2009 years).

138 The JWD has its advantage and disadvantages over the other disdrometers (Lee and
139 Zawadzki, 2005;McFarquhar and List, 1993;Sauvageot and Lacaux, 1995;Sheppard,
140 1990;Sheppard and Joe, 1994;Tokay et al., 2001;Tokay et al., 2013). For instance, JWD can't
141 measure fall velocity; hence, to evaluate the RSD parameters from the JWD, we assumed that
142 raindrops reach the ground with terminal velocity. Further, in heavy rainfall events, the JWD
143 measures the spurious values for the raindrops of diameter < 1 mm, and it was named as the
144 dead-time of the instrument. To deal with the dead-time of the JWD, the manufacturer provided
145 an error correction multiplication matrix based on a correction scheme from Sheppard and Joe
146 (1994). However, as the JWD can't record any drops for the first three to four channels in heavy
147 rainfall events, the multiplicative matrix algorithm does not increase the counts when the channel
148 has no drops (Tokay & Short, 1996; Tokay et al., 2001); hence, in this study, we didn't apply the
149 dead-time correction to the JWD data. On top of that, 1-min RSD samples with raindrops count $<$
150 10 and rainfall rate < 0.1 mm h⁻¹ were discarded (Tokay & Short, 1996). The daily rainfall
151 accumulations from the JWD are related to the collocated rain gauge for both TY and NTY rain
152 regimes and are illustrated with scatter plots in Fig.2. The rainy days (TY: 04 days and NTY: 0
153 days) with larger discrepancy between JWD and rain gauge measurements were discarded in this
154 study. Further, we compared the JWD measurements (for both TY and NTY rainy days) with the
155 rain gauge for different wind speed conditions (daily maximum wind speed: 0-8, 8-14, 14-18, $>$
156 18 m s⁻¹), and the results are provided in Table 1. For the considered NTY rainy days, the daily

157 maximum wind speeds were less than 14 m s^{-1} , however, there were TY rainy days with wind
158 speed $> 18 \text{ m/s}$. A good agreement between JWD and rain gauge measurements for both TY and
159 NTY days (Fig.2 and Table 1) provided the trustworthiness of the JWD data for further analysis.

160 The rain/RSD parameters like raindrop concentration $N(D)$ ($\text{mm}^{-1} \text{ m}^{-3}$), radar reflectivity
161 factor Z ($\text{mm}^6 \text{ m}^{-3}$), liquid water content W (g m^{-3}), rainfall rate R (mm h^{-1}), total number
162 concentration N_t (m^{-3}), normalized intercept parameter, N_w ($\text{m}^{-3} \text{ mm}^{-1}$), shape parameter μ (-),
163 slope parameter Λ (mm^{-1}), and mass-weighted mean diameter D_m (mm) are estimated from the
164 JWD measurements. The formulations for these rain/RSD parameters are detailed in Seela et al.
165 (2017);Seela et al. (2018);Tokay et al. (2001);Bringi et al. (2003);Tokay and Short (1996). Along
166 with rain parameters, the rainfall kinetic energy (KE), which can be expressed in KE flux (KE_{time} ,
167 in $\text{J m}^{-2} \text{ h}^{-1}$) and KE content (KE_{mm} , $\text{J m}^{-2} \text{ mm}^{-1}$) were computed for TY and NTY rainfall using
168 the procedures of Fornis et al. (2005);Salles et al. (2002);van Dijk et al. (2002).

169 In addition to disdrometer data, remote-sensing (TRMM and MODIS) and reanalysis
170 (ERA-interim) data sets are used to elucidate the thermodynamical and microphysical
171 characteristics that are accountable for the possible disparities in RSDs between TY and NTY
172 rainfall. Bright band and storm heights from TRMM satellite (2A23 data product) (Iguchi et al.,
173 2000;Kummerow et al., 2001), cloud effective radii (CER) of liquid and ice particles from
174 MODIS satellite (MOD08_D3 data product) (Platnick et al., 2015;Remer et al., 2005;Nakajima
175 and King, 1989), water vapor, convective available potential energy (CAPE), relative humidity
176 and temperature profiles from ERA-Interim (Dee et al., 2011) are considered for TY and NTY
177 rainfall. A brief description of these data sets can be found in Seela et al. (2017) Janapati et al.
178 (2020).

179 Besides remote-sensing and re-analysis data sets, the radar reflectivity profiles from
180 radars mosaic are used to reveal TY and NTY rainfall characteristics. The Z profiles were
181 obtained from the six ground-based radars, and the locations of these radars are depicted with red
182 triangles in Fig. 1. Over the JWD site, the reflectivity profiles available for the period of 2005-
183 2014 are used, and further details on Taiwan radar reflectivity mosaic can be found in Chang et
184 al. (2020).

185

186 **3. Observational Results**

187 The quality-controlled JWD data showed 23074 and 20368 minutes of RSD samples,
188 respectively, for TY and NTY rainfall, and the mean raindrops concentrations of these two
189 weather conditions are depicted in Fig. 3. In this work, raindrops of diameter greater than 3 mm,
190 1–3 mm, and less than 1 mm are named, respectively, as large, mid-size, and small drops (Tokay
191 et al., 2008; Seela et al., 2018). As illustrated in Fig. 3a, perceivable segregation between TY and
192 NTY rainfall RSDs can be seen with more large drops in NTY than the TY rainfall. Despite of
193 weak distinction between TY and NTY mean rain spectra for raindrops of diameter < 2 mm, it
194 can be seen that the spectra variability within TY and NTY classes is smaller than the differences
195 between averaged TY and NTY spectra. Given the dependency of raindrop concentration on
196 rainfall rate, it is difficult to interpret alterations between TY and NTY rainfall RSD from Fig.
197 3a. Consequently, we implemented the normalization procedure (Testud et al., 2001), which is
198 independent of the shape of the observed raindrop spectra, to the TY and NTY RSDs. For TY
199 and NTY rainfall, the drop diameter (D , mm) and raindrop concentrations [$N(D)$, $\text{mm}^{-1} \text{m}^{-3}$] are
200 normalized, respectively, by mass-weighted mean diameter (D_m , mm) and normalized intercept

201 parameter (N_w , $\text{mm}^{-1} \text{m}^{-3}$), and these normalized RSDs are illustrated in Fig. 3b. A remarkable
202 departure in the normalized RSDs spectra between NTY and TY rainfall (for $D/D_m > 2$)
203 insinuates that divergent microphysical processes were involved in these two weather conditions.

204 For TY and NTY rainfall, the probability density functions (PDFs) are evaluated for D_m
205 (mass-weighted mean diameter in mm), $\log_{10}N_w$ (N_w is normalized intercept parameter in mm^{-1}
206 m^{-3}), $\log_{10}R$ (R is rainfall rate in mm h^{-1}), and $\log_{10}W$ (W is the liquid water content in g m^{-3})
207 and are depicted in Fig. 4. Fig. 4a demonstrates the PDF of D_m in NTY rainfall has higher
208 distribution than TY rainfall for $D_m > 1.7$ mm. The $\log_{10}N_w$ ($\log_{10}R$) PDF distribution shows peak
209 values around 3.7 (0.3) and 3.4 (0), respectively, for TY and NTY rainfall (Fig. 4b &c). The PDF
210 of $\log_{10}W$ shows a higher percentage at lower $\log_{10}W$ values ($\log_{10}W < -1$) in NTY rainfall, and a
211 higher percentage at higher $\log_{10}W$ values ($\log_{10}W > -1$) in TY rainfall (Fig. 4d). Further, a
212 statistical Student's t-test (used to determine whether two data sets are significantly different
213 from each other or not), is executed between TY and NTY rainfall D_m values. The test results
214 rejected the null hypothesis at 0.05 and 0.01 significance levels, which confirm that the D_m
215 values in TY rainfall are different from that of the NTY rainfall. Similarly, the Student's t-test
216 performed for other three parameters ($\log_{10}N_w$, $\log_{10}R$, and $\log_{10}W$) also showed that these
217 parameters in TY rainfall are different from that of the NTY rainfall.

218

219 **3.1 Contribution of raindrop diameters to N_t and R**

220 The contributions of raindrop diameter classes (diameter < 1 mm, 1–2 mm, 2–3 mm, 3–4
221 mm, and 4–5 mm) to N_t (m^{-3}) and R (mm h^{-1}) for TY and NTY rainfall are shown in Fig. 5. As

222 can be seen in Fig.5a & b, for both TY and NTY rainfall, with the increase of drop diameter
 223 classes, contribution to total number concentration decreases, while that of rainfall rate increases
 224 and then lessens, and such peculiarities were noticed by previous researchers on tropical
 225 cyclones (Chen et al., 2019) and summer season rainfall (Wu et al., 2019). For both TY and
 226 NTY rainfall, small size drops (< 1 mm) grant to large number concentration (> 70%) and about
 227 10% to rainfall rate. For both TY and NTY rainfall, raindrops with diameter 1–2 mm afford
 228 around 20% to number concentration; nonetheless, these raindrops (1–2 mm) yield around 60%
 229 (55%) to rainfall rate for TY (NTY) rainfall. The contribution of raindrops with diameters 2–3
 230 mm to number concentration is negligible, and the rainfall rate is above 20% for both TY and
 231 NTY rainfall. Fig. 5a&b emphasize the predominant contribution of small (< 1 mm) and mid-
 232 size drops (1–3 mm) to total number concentration and rainfall rate than large drops. The
 233 occurrence percentages of N_t (m^{-3}) ($[(N_t)_{TY}$ or $(N_t)_{NTY}/((N_t)_{TY} + (N_t)_{NTY})] \times 100$) and R ($mm\ h^{-1}$)
 234 ($[(R)_{TY}$ or $(R)_{NTY}/((R)_{TY} + (R)_{NTY})] \times 100$) at different diameter classes are illustrated,
 235 respectively, in Fig.5c and Fig.5d. For the first three drop diameter classes (< 1 mm, 1–2 mm,
 236 2–3 mm), the N_t (m^{-3}) percentages are predominant in TY than NTY rainfall, and in contrast, for
 237 large drops (> 3 mm), the N_t (m^{-3}) percentages are higher in NTY than TY rainfall. Similar to the
 238 N_t (m^{-3}), the rainfall rate percentages are higher in TY than NTY rainfall for small and mid-size
 239 drops, and an opposite feature can be seen for large drops (> 3 mm).

240

241 3.2 Segregation of RSDs based on rainfall rates

242 To further explore the discrepancies between TY and NTY rainfall RSDs, we segregate
 243 the TY and NTY RSDs into seven rainfall rate classes (as given in Table 2) using the below-

244 mentioned grouping criteria. The data points in each rainfall rate category should be sufficiently
 245 large in TY and NTY rainfall, and for each category, the mean values of rainfall rates should be
 246 nearly equal between these two weather conditions (TY and NTY rainfall) (Jayalakshmi and
 247 Reddy, 2014;Deo and Walsh, 2016;Seela et al., 2017). Statistical values of these seven rainfall
 248 rate categories are specified in Table 2 for TY and NTY rainfall. As depicted in the table, the
 249 mean values of rainfall rates are nearly equal between these two weather conditions (TY and
 250 NTY). Excluding fourth and fifth rainfall rate class (C4 and C5), the skewness values are
 251 excessive in NTY than TY rainfall. Correspondingly, these two weather conditions (TY and
 252 NTY) show positive skewness designating that the rainfall rates are focused on the left to the
 253 mean. The RSDs peculiarities between TY and NTY rainfall are evaluated in percentage
 254 parameter (Ratio of $N(D)$ in TY or NTY rainfall for the raindrop diameter D and rainfall rate
 255 class R to the raindrop concentration accumulations in TY and NTY rainfall) context, as
 256 explicated in Seela et al. (2018). The percentage parameter of $N(D)$ for different rain rate class,
 257 $\delta(D, R) = \delta(D, R_{Ck})_{TY/NTY}$ is given as

$$258 \quad \delta(D, R_{Ck})_{TY} = \frac{[N(D)_{TY}]_{Ck}}{([N(D)_{TY}]_{Ck} + [N(D)_{NTY}]_{Ck})} \times 100 \quad \text{-----}(1)$$

$$259 \quad \delta(D, R_{Ck})_{NTY} = \frac{[N(D)_{NTY}]_{Ck}}{([N(D)_{TY}]_{Ck} + [N(D)_{NTY}]_{Ck})} \times 100 \quad \text{-----}(2)$$

260 Where $[N(D)_{TY}]_{Ck}$ or $[N(D)_{NTY}]_{Ck}$ represents the mean $N(D)$ of TY or NTY rainfall for the
 261 rain rate class “Ck”, with k=1, 2, 3, 4, 5, 6, 7 (C1: $0.1 \leq R < 1$, C2: $1 \leq R < 2$, C3: $2 \leq R < 5$, C4:
 262 $5 \leq R < 10$, C5: $10 \leq R < 30$, C6: $30 \leq R < 50$, and C7: $R > 50$, where R is in mm h^{-1} ; please refer
 263 to table 2).

264 The raindrop concentration percentages are appraised for both TY and NTY rainfall and are
265 illustrated in Fig. 6. The percentage contribution of $N(D)$ for TY and NTY rainfall corroborated
266 that small and mid-size drops (< 3 mm) display superior percentage in TY than NTY rainfall.
267 Nevertheless, large drops (> 3 mm) unveil a higher percentage of $N(D)$ in NTY than TY rainfall.

268 Distributions of D_m (mm) and $\log_{10}N_w$ ($\text{m}^{-3} \text{mm}^{-1}$) for seven rainfall rate classes are
269 depicted with box plots in Fig. 7. As can be seen from Fig. 7a, with the increase in rainfall rate
270 class, D_m values increase for both TY and NTY rainfall, which is due to a raise in large size
271 drops concentration and a reduction in small drops concentration (Rosenfeld and Ulbrich,
272 2003; Krishna et al., 2016), and similar finding were noticed by previous researchers for both
273 tropical cyclones and non-tropical cyclones rainfall (Bao et al., 2020; Deo and Walsh,
274 2016; Jayalakshmi and Reddy, 2014; Radhakrishna and Narayana Rao, 2010). On the other hand,
275 D_m values are greater in NTY than TY rainfall in all rainfall rate classes due to the predominant
276 concentration of mid-size and small-size raindrops in TY than NTY days (Fig.6). Compared to
277 D_m , for all seven rainfall rate classes, the $\log_{10}N_w$ values are higher in TY than NTY rainfall
278 (Fig.7b).

279

280 **3.3 RSDs in precipitation types**

281 Ample literature showed distinctiveness in the RSDs with precipitation type, and
282 numerous methods were documented to segregate the precipitation into stratiform and
283 convective type (Ma et al., 2019; Jayalakshmi and Reddy, 2014; Ulbrich and Atlas, 2007). For
284 instance, Tokay and Short (1996) reported variations in convective precipitations to that of the

285 stratiform regimes. Some studies emphasized the importance to adopt precipitation specific
286 rainfall estimation relations (Ulbrich and Atlas, 2007). In separating the TY and NTY rainfall
287 into stratiform and convective type, we adopted the modified form of Bringi et al. (2003)
288 classification method as mentioned in Ma et al. (2019). Distributions of mean $N(D)$ ($\text{m}^{-3} \text{mm}^{-1}$)
289 with raindrop diameters for TY and NTY rainfall are depicted in Fig. 8a. Except for the first drop
290 size bin, higher drop concentrations are noticed for convective rainfall than the stratiform
291 rainfall. Concave shaped $N(D)$ with broader distribution in convective than stratiform is due to
292 the breakup of large drops by collisions (Hu and Srivastava, 1995). The RSD characteristics
293 demonstrated by the stratiform and convective precipitations show similar features to that of the
294 earlier studies for continental (Jayalakshmi and Reddy, 2014) and oceanic regions (Krishna et al.,
295 2016). On the other hand, in stratiform and convective regimes, the mid-size and large drops
296 concentration is higher in NTY than TY rainfall. Variations in D_m and $\log_{10}N_w$ for both
297 precipitations of TY and NTY are depicted in Fig. 8b. The maritime and continental convective
298 clusters of Bringi et al. (2003) are depicted with gray rectangles. For both TY and NTY rainfall,
299 larger mean D_m and $\log_{10}N_w$ values are noticed for convective precipitation. In contrast to that, in
300 stratiform and convective regimes, the NTY rainfall exhibit smaller $\log_{10}N_w$ and larger D_m values
301 than TY rainfall.

302

303 **3.4 Rainfall estimation relations**

304 Uncertainties in the estimation of rainfall from weather radars can be minimized through
305 region, weather system, and precipitation specific radar reflectivity and rainfall rate ($Z-R$)
306 relations. In $Z = A R^b$ relation, size of the raindrops can be inferred from the coefficient 'A', and

307 the exponent ‘b’ represents microphysical process (Atlas et al., 1999;Steiner et al., 2004;Atlas
308 and Williams, 2003). The TY and NTY rainfall $Z-R$ relations are derived from the linear
309 regression applied to $10*\log_{10}R$, and Z , and are provided in Fig. 09. The coefficient values of
310 $Z-R$ relations are larger in NTY than the TY for stratiform and convective precipitations, as well
311 as for total rainfall. This variation is due to the presence of significant number of large-size drops
312 in NTY to that of the TY rainfall. The current TY rainfall $Z-R$ relations show disparity with the
313 other locations tropical cyclones rainfall relations (Bao et al., 2020;Wen et al., 2018;Janapati et
314 al., 2020). The possible reasons for the variations in other locations' tropical
315 cyclones $Z-R$ relations to that of the present TY rainfall could be due to geographical variations
316 or the RSD measurements from different types of disdrometers (Adirosi et al., 2018). Moreover,
317 the obtained TY and NTY days $Z-R$ relations are found to differ from the default ($Z=300 R^{1.4}$)
318 and tropical $Z-R$ relationships ($Z=250R^{1.2}$), which suggests to adopt weather and region-specific
319 $Z-R$ relations.

320

321 **3.5 The rainfall rate relationships with D_m and N_w**

322 The normalized intercept parameter and mass-weighted mean diameter values can
323 provide the RSD features, and these parameters were found to show uniqueness with the rainfall
324 rate (Chen et al., 2016;Janapati et al., 2020). Distribution of D_m and $\log_{10}N_w$ with rainfall rates
325 for both weather conditions are portrayed in Fig. 10. As can be seen from the figure, the
326 distributions of D_m gets narrowed with the increase in rainfall rates for both weather conditions,
327 and such behaviors were reported for tropical cyclone and summer season rainfall (Kumar and
328 Reddy, 2013;Wen et al., 2018;Chang et al., 2009;Janapati et al., 2020;Chen et al., 2019;Wu et

329 al., 2019). No further fluctuations in the D_m values at higher rainfall rates ($> 25 \text{ mm h}^{-1}$) are due
330 to the equilibrium condition in the RSDs (attained through raindrop breakup and coalescence
331 processes) (Hu and Srivastava, 1995), and further increase in rainfall rates is due to the increase
332 in number concentration under RSDs equilibrium condition (Bringi and Chandrasekar, 2001).
333 The power-law equations for D_m-R and $\log_{10}N_w-R$ are computed using a non-linear least squares
334 method and are exemplified in Fig. 10. The evaluated D_m-R ($\log_{10}N_w-R$) relations exhibit a
335 larger (smaller) coefficient in NTY rainfall than TY rainfall, which confirm that for given
336 rainfall rates, the NTY rainfall had a higher D_m and lower N_w values than the TY rainfall.

337

338 **3.6 $KE-R$ and $KE-D_m$ relations**

339 The raindrops reaching the ground with a certain amount of kinetic energy (KE) can
340 erode the soil from the ground surface. Hence, the raindrops KE or rainfall KE is one of the
341 critical physical quantities in soil erosion studies (Wischmeier, 1959;Kinnell, 1981). As the
342 rainfall KE is related to the raindrop diameter and its fall velocity, it can be evaluated through the
343 RSD information (Kinnell, 1981). The empirical relations between the rainfall KE and rainfall
344 intensity are incorporated in assessing the rainfall erosivity factor (R-factor), one of the key
345 parameters in soil erosion modeling studies (Renard et al., 1997;Janapati et al., 2019). To this
346 end, we investigated the empirical relations between the rainfall KE (KE_{time} in $\text{J m}^{-2} \text{ h}^{-1}$; KE_{mm} in
347 $\text{J m}^{-2} \text{ mm}^{-1}$) and rainfall rate (mm h^{-1}) using non-linear least-squares regression method for TY
348 and NTY rainfall. The distribution plots of KE_{mm} and KE_{time} with R for TY and NTY rainfall are
349 portrayed in Fig. 11. The $KE_{time}-R$ empirical relations are derived by fitting the data points with
350 power and liner methods. For both TY and NTY days, the power-law line fitted well by passing

351 through the middle of the data points at both lower and higher rainfall rates than the linear fit line
352 (Fig. 11a & b). The KE_{mm} and R data points are fitted with power, logarithmic, and exponential
353 law. Among three forms of relations, the power-law fitted well with the data points for both TY
354 and NTY days (Fig. 11c & d). Moreover, empirical relations between D_m (mm), the KE_{mm} are
355 evaluated for both TY and NTY rainfall and are given in Fig. 12. Comparison of present $KE-D_m$
356 relations with the East China seasonal rainfall $KE-D_m$ ($KE = -2.33D_m^2 + 21.05D_m - 7.79$) relation
357 shows that both TY and NTY relations in Taiwan are different from that of East China (Wen et
358 al., 2019). The derived $KE-D_m$ relations can be used to estimate the KE values from the remote-
359 sensing radar (GPM DPR) measurements. The $KE_{time}-R$, $KE_{mm}-R$, and $KE-D_m$ relations and their
360 statistical values are given in Table 3. For both $KE_{time}-R$, $KE_{mm}-R$ relations, the power-law
361 exhibits higher CC and lower RMSE and NRMSE values, which suggest to adopt the power
362 form equation to estimate the rainfall KE .

363

364 4. Discussion

365 To apprehend propitious mechanisms responsible for the discrepancies in RSDs between
366 TY and NTY rainfall, re-analysis, remote sensing, and ground-based radar data sets are used.
367 The water vapor and CAPE values for TY and NTY days depicted with a box plot in Fig. 13
368 signify that NTY days had strong convective activity with vigorous updrafts and downdrafts than
369 TY days. Nonetheless, if we look at the storm and bright band heights (BBH) (Fig. 14), TY days
370 had relatively higher BBH than NTY days and there are no apparent alterations in storm heights
371 between TY and NTY days. Relatively higher BBH support the greater CER values for ice
372 particles in TY than NTY days (Fig. 15b). Nevertheless, there is no much difference in the liquid

373 particles CER median values between TY and NTY days (Fig.15a). The deep stratiform clouds
374 in TY days offer sufficient time for the growth of ice crystals to large size (via aggregation and
375 vapor deposition) and melt to big size drops once they cross the melting layer. Relatively higher
376 BBH in TY days allowed the RSDs to reach equilibrium through various microphysical
377 processes (collision, coalescence, and breakup) than NTY rainfall (Hu and Srivastava, 1995). In
378 contrast, intense convection (with resilient updrafts and downdrafts) in NTY days enhances
379 raindrops growth (through collision-coalescence and drop sorting processes), shoots smaller
380 drops at higher altitudes, and allows large drops to reach the surface. The vertical profiles of air
381 temperature and relative humidity for TY and NTY days evidently illustrate that NTY days were
382 drier compared to that of the TY rainy days (Fig. 16), and hence, the rate of evaporation of small
383 drops (that were produced through the collision breakup processes) in NTY days was higher than
384 TY days resulting in more large drops in NTY days.

385
386 The radar reflectivity CFAD (contoured frequency-by-altitude diagrams) for (a) typhoon
387 (TY) and (b) non-typhoon (NTY) days are portrayed in Fig. 17. The vertical sky blue (dark
388 magenta) star line in Fig. 17a (Fig.17b) is the mean radar reflectivity profile of TY (NTY) days.
389 The white-star dotted profile in Fig.17a & b is the mean of both TY and NTY days' reflectivity
390 profiles. The mean reflectivity profile of TY (NTY) days is less (higher) than the mean of TY
391 and NTY days' reflectivity profile. A higher occurrence percentage of lower Z values ($Z < 10$
392 dBZ) in TY than NTY days can be seen at higher altitudes. In contrast to that, below the melting
393 layer, the occurrence percentage of higher reflectivity values ($Z > 40$ dBZ) is higher in NTY than
394 TY days. The mean vertical profiles of radar reflectivity for TY and NTY days are plotted in Fig.
395 18. It can be seen from the figure that the mean reflectivity values are higher in NTY than TY

396 days. As the radar reflectivity is directly related to the sixth power of raindrop diameter, higher
397 reflectivity profiles in NTY than TY days infer the predominance of large drops in NTY than TY
398 rainy days. The above-mentioned microphysical and thermodynamical processes resulted in
399 more big size drops and few small drops in NTY than TY days, resulting in higher D_m and lower
400 N_w values in NTY than TY days.

401

402 **5. Summary and conclusions**

403 Raindrop size distributions (RSDs) of typhoon (TY) and non-typhoon (NTY) rainy days
404 have been analyzed using long-term (2004-2016) disdrometer measurements from north Taiwan.
405 Besides disdrometer data, other auxiliary data sets (remote-sensing, re-analysis, and ground-
406 based radar) have been used to discuss the disparities in RSDs between TY and NTY rainfall.
407 The NTY days have more big-size drops and less small-size drops than TY days, resulting in
408 larger D_m and smaller N_w values in NTY days. The mean normalized RSD of NTY precipitation
409 has a higher occurrence of larger drops (at $D/D_m > 2$) than TY precipitation, which indicates the
410 possibility for diverse microphysical processes between these two weather conditions. The
411 classification of RSDs to varying rainfall rates and precipitation (stratiform and convective)
412 regimes clearly show smaller D_m and larger N_w values in TY than NTY days. The percentage
413 contribution of large (small and mid-size) drops to N_t and R is lower (higher) in TY than NTY
414 rainfall. For both TY and NTY rainy days, stratiform precipitations D_m and N_w values are smaller
415 than the maritime and continental clusters, while, convective precipitations D_m values are
416 approximately within the range of maritime clusters. The rainfall kinetic energy and intensity
417 (KE_{time-R} and KE_{mm-R}) relations evaluated for both TY and NTY rainy days reveal greater
418 performance of power relation than other types, and confirms to use power form of $KE-R$

419 relations in assessing the rainfall erosivity factor for TY and NTY rainfall events. The
420 enumerated $Z-R$, D_m-R , N_w-R , $KE_{time}-R$, $KE_{mm}-R$, and $KE_{mm}-D_m$ relations showed profound
421 diversity between TY and NTY rainfall and substantiate the significance of adopting
422 precipitation specific empirical relations in evaluating the rainfall rate and kinetic energy values.
423 Overall, present study confirms that relatively higher convective activity with drier conditions in
424 NTY than TY days significantly wedged the disparities in RSDs with dissimilar microphysical
425 processes. The current observational outcomes could benefit in appraising the radar precipitation
426 estimation algorithms, cloud modeling, and rainfall erosivity in north Taiwan for TY and NTY
427 rainfall events.

428

429 *Data availability.* The Era-interim re-analysis data can be obtained from
430 <https://www.ecmwf.int/en/forecasts/datasets/reanalysis-datasets/era-interim>. The TRMM data
431 can be retrieved from <https://gpm.nasa.gov/data/directory>. The MODIS cloud data product can
432 be accessed through <https://modis.gsfc.nasa.gov/data/dataproduct/mod06.php>. The ground-based
433 radar and disdrometer data are available from the corresponding author upon reasonable request.

434

435 *Author contributions.* JJ and BKS conceptualized the idea; PLL and EJ provided funding
436 acquisition, project administration, and observation data; JJ, BKS, and MTL conducted the
437 detailed analysis; PLL, and EJ supervised the analysis; JJ, BKS wrote the initial manuscript; JJ,
438 BKS, PLL reviewed and revised the manuscript; all authors involved in writing the manuscript
439 and revisions.

440

441 *Competing interests.* No conflict of interest is declared by the all authors.

442

443 *Acknowledgements.* We acknowledge the Central Weather Bureau (CWB) of Taiwan, in
444 facilitating the radar reflectivity data, and Tropical Rainfall Measuring Mission (TRMM), ERA-
445 Interim and MODIS research team for their efforts in providing the data. This research work is
446 carried out under the Taiwan Ministry of Science and Technology (MOST) grant numbers:
447 MOST 108-2111-M-008-028, MOST 108-2625-M-008-011, MOST: 104-2923-M-008-003 and
448 partially by “Earthquake-Disaster & Risk Evaluation and Management Center, E-DREaM” from
449 The Featured Areas Research Center Program within the framework of the Higher Education
450 Sprout Project by the Ministry of Education (MOE), Taiwan. The first author, JJ is supported by
451 the grant number MOST 108–2811–M–008–558, and second author, BKS, by MOST 108-2625-
452 M-008-011 and MOST 108-2811-M-008-595.

453 References

454

455 Adirosi, E., Roberto, N., Montopoli, M., Gorgucci, E., and Baldini, L.: Influence of Disdrometer
456 Type on Weather Radar Algorithms from Measured DSD: Application to Italian
457 Climatology, *Atmosphere-Basel*, 9, 360, 10.3390/atmos9090360, 2018.

458 Atlas, D., Ulbrich, C. W., Marks Jr, F. D., Amitai, E., and Williams, C. R.: Systematic variation
459 of drop size and radar-rainfall relations, *Journal of Geophysical Research: Atmospheres*,
460 104, 6155-6169, 10.1029/1998JD200098, 1999.

461 Atlas, D., and Williams, C. R.: The Anatomy of a Continental Tropical Convective Storm,
462 *Journal of the Atmospheric Sciences*, 60, 3-15, 10.1175/1520-
463 0469(2003)060<0003:TAOACT>2.0.CO;2, 2003.

464 Bao, X., Wu, L., Zhang, S., Li, Q., Lin, L., Zhao, B., Wu, D., Xia, W., and Xu, B.: Distinct
465 Raindrop Size Distributions of Convective Inner- and Outer-Rainband Rain in Typhoon
466 Maria (2018), *Journal of Geophysical Research: Atmospheres*, 125, e2020JD032482,
467 10.1029/2020jd032482, 2020.

468 Bringi, V. N., and Chandrasekar, V.: *Polarimetric Doppler Weather Radar: Principles and*
469 *Applications*, Cambridge University Press., 2001.

470 Bringi, V. N., Chandrasekar, V., Hubbert, J., Gorgucci, E., Randeu, W. L., and Schoenhuber, M.:
471 Raindrop Size Distribution in Different Climatic Regimes from Disdrometer and Dual-
472 Polarized Radar Analysis, *Journal of the Atmospheric Sciences*, 60, 354-365,
473 10.1175/1520-0469(2003)060<0354:RSDIDC>2.0.CO;2, 2003.

474 Chang, J. M., Chen, H. E., Jou, B. J. D., Tsou, N. C., and Lin, G. W.: Characteristics of Rainfall
475 Intensity, Duration, and Kinetic Energy for Landslide Triggering in Taiwan, *Engineering*
476 *Geology*, 231, 81-87, 10.1016/j.enggeo.2017.10.006, 2017.

477 Chang, P.-L., Zhang, J., Tang, Y.-S., Tang, L., Lin, P.-F., Langston, C., Kaney, B., Chen, C.-R.,
478 and Howard, K.: An Operational Multi-Radar Multi-Sensor QPE System in Taiwan,
479 *Bulletin of the American Meteorological Society*, 1-56, 10.1175/bams-d-20-0043.1, 2020.

480 Chang, W.-Y., Wang, T.-C. C., and Lin, P.-L.: Characteristics of the Raindrop Size Distribution
481 and Drop Shape Relation in Typhoon Systems in the Western Pacific from the 2D Video
482 Disdrometer and NCU C-Band Polarimetric Radar, *Journal of Atmospheric and Oceanic*
483 *Technology*, 26, 1973-1993, 10.1175/2009jtecha1236.1, 2009.

484 Chen, B., Wang, J., and Gong, D.: Raindrop size distribution in a midlatitude continental squall
485 line measured by thies optical disdrometers over East China, *J. Appl. Meteor. Climatol.*,
486 55, 621–634, 10.1175/JAMC-D-15-0127.1, 2016.

487 Chen, C.-S., and Chen, Y.-L.: The Rainfall Characteristics of Taiwan, *Monthly Weather Review*,
488 131, 1323-1341, 10.1175/1520-0493(2003)131<1323:trcot>2.0.co;2, 2003.

489 Chen, C.-S., Chen, Y.-L., Liu, C.-L., Lin, P.-L., and Chen, W.-C.: Statistics of Heavy Rainfall
490 Occurrences in Taiwan, *Weather and Forecasting*, 22, 981-1002, 10.1175/waf1033.1, 2007.

491 Chen, G., Zhao, K., Zhang, G., Huang, H., Liu, S., Wen, L., Yang, Z., Yang, Z., Xu, L., and Zhu,
492 W.: Improving Polarimetric C-Band Radar Rainfall Estimation with Two-Dimensional
493 Video Disdrometer Observations in Eastern China, *Journal of Hydrometeorology*, 18,
494 1375-1391, 10.1175/jhm-d-16-0215.1, 2017.

495 Chen, J.-M., Li, T., and Shih, C.-F.: Tropical Cyclone– and Monsoon-Induced Rainfall
496 Variability in Taiwan, *Journal of Climate*, 23, 4107-4120, 10.1175/2010jcli3355.1, 2010.

497 Chen, J.-M., and Chen, H.-S.: Interdecadal Variability of Summer Rainfall in Taiwan Associated
498 with Tropical Cyclones and Monsoon, *Journal of Climate*, 24, 5786-5798,
499 10.1175/2011jcli4043.1, 2011.

500 Chen, K., Chu, C.-Y., and Tzeng, Y.-C.: A semi-empirical model of rain attenuation at Ka-band
501 in Northern Taiwan, *Progress In Electromagnetics Research*, 16, 213-223, 2011.

502 Chen, T.-C., Yen, M.-C., Hsieh, J.-C., and Arritt, R. W.: Diurnal and Seasonal Variations of the
503 Rainfall Measured by the Automatic Rainfall and Meteorological Telemetry System in
504 Taiwan, *Bulletin of the American Meteorological Society*, 80, 2299-2312, 10.1175/1520-
505 0477(1999)080<2299:Dasvot>2.0.Co;2, 1999.

506 Chen, Y., Duan, J., An, J., and Liu, H.: Raindrop Size Distribution Characteristics for Tropical
507 Cyclones and Meiyu-Baiu Fronts Impacting Tokyo, Japan, *Atmosphere-Basel*, 10, 391,
508 2019.

509 Chu, P.-S., Zhao, X., Lee, C.-T., and Lu, M.-M.: Climate prediction of tropical cyclone activity
510 in the vicinity of Taiwan using the multivariate least absolute deviation regression method,
511 *Terrestrial Atmospheric and Oceanic Sciences*, 18, 805, 2007.

512 Chu, Y.-H., and Su, C.-L.: An Investigation of the Slope–Shape Relation for Gamma Raindrop
513 Size Distribution, *Journal of Applied Meteorology and Climatology*, 47, 2531-2544,
514 10.1175/2008jamc1755.1, 2008.

515 Dee, D. P., Uppala, S., Simmons, A., Berrisford, P., Poli, P., Kobayashi, S., Andrae, U.,
516 Balsameda, M., Balsamo, G., and Bauer, d. P.: The ERA-Interim Reanalysis:
517 Configuration and Performance of the Data Assimilation System, *Quarterly Journal of the*
518 *royal meteorological society*, 137, 553-597, 2011.

519 Deo, A., and Walsh, K. J.: Contrasting tropical cyclone and non-tropical cyclone related rainfall
520 drop size distribution at Darwin, Australia, *Atmospheric Research*, 181, 81-94, 2016.

521 Fornis, R. L., Vermeulen, H. R., and Nieuwenhuis, J. D.: Kinetic Energy–Rainfall Intensity
522 Relationship For Central Cebu, Philippines for Soil Erosion Studies, *Journal of*
523 *Hydrology*, 300, 20-32, 10.1016/j.jhydrol.2004.04.027, 2005.

524 Hu, Z., and Srivastava, R. C.: Evolution of Raindrop Size Distribution by Coalescence, Breakup,
525 and Evaporation: Theory and Observations, *Journal of the Atmospheric Sciences*, 52,
526 1761-1783, 10.1175/1520-0469(1995)052<1761:Eorsdb>2.0.Co;2, 1995.

527 Iguchi, T., Kozu, T., Meneghini, R., Awaka, J., and Okamoto, K. i.: Rain-Profiling Algorithm for
528 the TRMM Precipitation Radar, *Journal of Applied Meteorology*, 39, 2038-2052,
529 10.1175/1520-0450(2001)040<2038:RPAFTT>2.0.CO;2, 2000.

530 Janapati, J., Reddy, V., Reddy, K., Lin, P.-L., and Liu, C.-Y.: A study on raindrop size
531 distribution variability in before and after landfall precipitations of tropical cyclones
532 observed over southern India, *Journal of Atmospheric and Solar-Terrestrial Physics*, 159,
533 23-40, 2017.

534 Janapati, J., Seela, B. K., Lin, P.-L., Wang, P. K., and Kumar, U.: An assessment of tropical
535 cyclones rainfall erosivity for taiwan, *Scientific reports*, 9, 15862, 2019.

536 Janapati, J., Seela, B. K., Lin, P.-L., Wang, P. K., Tseng, C.-H., Reddy, K. K., Hashiguchi, H.,
537 Feng, L., Das, S. K., and Unnikrishnan, C. K.: Raindrop Size Distribution Characteristics
538 of Indian and Pacific Ocean Tropical Cyclones Observed at India and Taiwan Sites,
539 *Journal of the Meteorological Society of Japan. Ser. II*, 98, 299-317, 10.2151/jmsj.2020-
540 015, 2020.

541 Jayalakshmi, J., and Reddy, K. K.: Raindrop size distributions of southwest and northeast
542 monsoon heavy precipitation observed over Kadapa (14°4'N, 78°82'E), a semi-arid region
543 of India, *Current Science*, 107, 1312-1320, 2014.

544 Joss, J., and Waldvogel, A.: Raindrop Size Distribution and Sampling Size Errors, *Journal of the*
545 *Atmospheric Sciences*, 26, 566-569, 10.1175/1520-0469(1969)026<0566:rsdass>2.0.co;2,
546 1969.

547 Jung, S.-A., Lee, D.-I., Jou, B. J.-D., and Uyeda, H.: Microphysical Properties of Maritime
548 Squall Line Observed on June 2, 2008 in Taiwan, *Journal of the Meteorological Society of*
549 *Japan. Ser. II*, 90, 833-850, 10.2151/jmsj.2012-516, 2012.

550 Kinnell, P. I. A.: Rainfall Intensity-Kinetic Energy Relationships for Soil Loss Prediction1, *Soil*
551 *Science Society of America Journal*, 45, 153-155,
552 10.2136/sssaj1981.03615995004500010033x, 1981.

553 Krishna, U. V. M., Reddy, K. K., Seela, B. K., Shirooka, R., Lin, P.-L., and Pan, C.-J.: Raindrop
554 size distribution of easterly and westerly monsoon precipitation observed over Palau
555 islands in the Western Pacific Ocean, *Atmospheric Research*, 174-175, 41-51,
556 <https://doi.org/10.1016/j.atmosres.2016.01.013>, 2016.

557 Kumar, S. B., and Reddy, K. K.: Rain drop size distribution characteristics of cyclonic and north
558 east monsoon thunderstorm precipitating clouds observed over Kadapa (14.47°N,
559 78.82°E), tropical semi-arid region of India, *Mausam*, 64, 35–48, 2013.

560 Kumari, N., Kumar, S. B., Jayalakshmi, J., and Reddy, K. K.: Raindrop size distribution
561 variations in JAL and NILAM cyclones induced precipitation observed over Kadapa
562 (14.47 ° N, 78.82 ° E), a tropical semi-arid region of India, *Indian Journal of Radio and*
563 *Space Physics*, 43, 57–66, 2014.

564 Kummerow, C., Hong, Y., Olson, W. S., Yang, S., Adler, R. F., McCollum, J., Ferraro, R., Petty,
565 G., Shin, D. B., and Wilheit, T. T.: The Evolution of the Goddard Profiling Algorithm
566 (GPROF) for Rainfall Estimation from Passive Microwave Sensors, *Journal of Applied*
567 *Meteorology*, 40, 1801-1820, 10.1175/1520-0450(2001)040<1801:TEOTGP>2.0.CO;2,
568 2001.

569 Lee, G. W., and Zawadzki, I.: Variability of Drop Size Distributions: Noise and Noise Filtering
570 in Disdrometric Data, *Journal of Applied Meteorology*, 44, 634-652, 10.1175/JAM2222.1,
571 2005.

572 Lee, M.-T., Lin, P.-L., Chang, W.-Y., Seela, B. K., and Janapati, J.: Microphysical
573 Characteristics and Types of Precipitation for Different Seasons over North Taiwan,
574 *Journal of the Meteorological Society of Japan. Ser. II*, 97, 841-865, 10.2151/jmsj.2019-
575 048, 2019.

576 Liang, A., Oey, L., Huang, S., and Chou, S.: Long-term trends of typhoon-induced rainfall over
577 Taiwan: In situ evidence of poleward shift of typhoons in western North Pacific in recent
578 decades, *Journal of Geophysical Research: Atmospheres*, 122, 2750-2765,
579 10.1002/2017jd026446, 2017.

580 Liao, L., Meneghini, R., and Tokay, A.: Uncertainties of GPM DPR Rain Estimates Caused by
581 DSD Parameterizations, *Journal of Applied Meteorology and Climatology*, 53, 2524-2537,
582 10.1175/JAMC-D-14-0003.1, 2014.

583 Lin, G.-W., and Chen, H.: The relationship of rainfall energy with landslides and sediment
584 delivery, *Engineering geology*, 125, 108-118, 2012.

585 Lu, J.-Y., Su, C.-C., Lu, T.-F., and Maa, M.-M.: Number and volume raindrop size distributions
586 in Taiwan, *Hydrological Processes*, 22, 2148-2158, 10.1002/hyp.6814, 2008.

587 Ma, Y., Ni, G., Chandra, C. V., Tian, F., and Chen, H.: Statistical characteristics of raindrop size
588 distribution during rainy seasons in the Beijing urban area and implications for radar
589 rainfall estimation, *Hydrology and Earth System Sciences*, 23, 4153-4170, 2019.

590 Maki, M., Keenan, T. D., Sasaki, Y., and Nakamura, K.: Characteristics of the Raindrop Size
591 Distribution in Tropical Continental Squall Lines Observed in Darwin, Australia, *Journal*
592 *of Applied Meteorology*, 40, 1393-1412, 10.1175/1520-
593 0450(2001)040<1393:COTRSD>2.0.CO;2, 2001.

594 McFarquhar, G. M., and List, R.: The Effect of Curve Fits for the Disdrometer Calibration on
595 Raindrop Spectra, Rainfall Rate, and Radar Reflectivity, *Journal of Applied Meteorology*,
596 32, 774-782, 10.1175/1520-0450(1993)032<0774:TEOCFF>2.0.CO;2, 1993.

597 McFarquhar, G. M., Hsieh, T.-L., Freer, M., Mascio, J., and Jewett, B. F.: The characterization
598 of ice hydrometeor gamma size distributions as volumes in $N \ 0-\lambda-\mu$ phase space:
599 Implications for microphysical process modeling, *Journal of the Atmospheric Sciences*, 72,
600 892-909, 2015.

601 Nakajima, T., and King, M. D.: Determination of the Optical Thickness and Effective Particle
602 Radius of Clouds from Reflected Solar Radiation Measurements. Part I: Theory, *Journal of*
603 *the Atmospheric Sciences*, 47, 1878-1893, 10.1175/1520-
604 0469(1990)047<1878:DOTOTA>2.0.CO;2, 1989.

605 Nakamura, K., and Iguchi, T.: Dual-wavelength Radar Algorithm, in: *Measuring precipitation*
606 *from space*, Springer, 225-234, 2007.

607 Platnick, S., King, M., and Hubanks, P.: MODIS Atmosphere L3 Daily Product, NASA MODIS
608 Adaptive Processing System, Goddard Space Flight Center, in, 2015.

609 Radhakrishna, B., and Narayana Rao, T.: Differences in cyclonic raindrop size distribution from
610 southwest to northeast monsoon season and from that of noncyclonic rain, *Journal of*
611 *Geophysical Research: Atmospheres*, 115, 10.1029/2009jd013355, 2010.

612 Remer, L. A., Kaufman, Y. J., Tanré, D., Mattoo, S., Chu, D. A., Martins, J. V., Li, R. R.,
613 Ichoku, C., Levy, R. C., Kleidman, R. G., Eck, T. F., Vermote, E., and Holben, B. N.: The
614 MODIS Aerosol Algorithm, Products, and Validation, *Journal of the Atmospheric*
615 *Sciences*, 62, 947-973, 10.1175/JAS3385.1, 2005.

616 Renard, K. G., Foster, G. R., Weesies, G. A., McCool, D. K., and Yoder, D. C.: Predicting Soil
617 Erosion by Water: A Guide to Conservation Planning with the Revised Universal Soil Loss
618 Equation (RUSLE) (Agricultural Handbook 703). US Department of Agriculture,
619 Washington, DC., 1997.

620 Rosenfeld, D., and Ulbrich, C. W.: Cloud Microphysical Properties, Processes, and Rainfall
621 Estimation Opportunities, *Meteorological Monographs*, 52, 237-258, 10.1175/0065-
622 9401(2003)030<0237:CMPPAR>2.0.CO;2, 2003.

623 Ryzhkov, A. V., and Zrnić, D. S.: Comparison of Dual-Polarization Radar Estimators of Rain,
624 *Journal of Atmospheric and Oceanic Technology*, 12, 249-256, 10.1175/1520-
625 0426(1995)012<0249:CODPRE>2.0.CO;2, 1995.

626 Salles, C., Poesen, J., and Sempere-Torres, D.: Kinetic Energy of Rain and Its Functional
627 Relationship With Intensity, *Journal of Hydrology*, 257, 256-270, 10.1016/S0022-
628 1694(01)00555-8, 2002.

629 Sauvageot, H., and Lacaux, J.-P.: The Shape of Averaged Drop Size Distributions, *Journal of the*
630 *Atmospheric Sciences*, 52, 1070-1083, 10.1175/1520-
631 0469(1995)052<1070:TSOADS>2.0.CO;2, 1995.

632 Seela, B. K., Reddy, K. K., Jayalakshmi, J., Rao, T. N., Lin, P.-L., Liu, C.-Y., and Kumar, U.:
633 Precipitation and cloud microstructure variations between two southern Indian stations,
634 Remote Sensing of the Atmosphere, Clouds, and Precipitation VI, 2016, 98761O,
635 Seela, B. K., Janapati, J., Lin, P. L., Reddy, K. K., Shirooka, R., and Wang, P. K.: A Comparison
636 Study of Summer Season Raindrop Size Distribution Between Palau and Taiwan, Two
637 Islands in Western Pacific, J Geophys Res-Atmos, 122, 11787-11805,
638 10.1002/2017jd026816, 2017.

639 Seela, B. K., Janapati, J., Lin, P.-L., Wang, P. K., and Lee, M.-T.: Raindrop Size Distribution
640 Characteristics of Summer and Winter Season Rainfall Over North Taiwan, Journal of
641 Geophysical Research: Atmospheres, 123, 11,602-611,624, 10.1029/2018jd028307, 2018.

642 Sheppard, B. E.: Effect of Irregularities in the Diameter Classification of Raindrops by the Joss-
643 Waldvogel Disdrometer, Journal of Atmospheric and Oceanic Technology, 7, 180-183,
644 10.1175/1520-0426(1990)007<0180:EOIITD>2.0.CO;2, 1990.

645 Sheppard, B. E., and Joe, P. I.: Comparison of Raindrop Size Distribution Measurements by a
646 Joss-Waldvogel Disdrometer, a PMS 2DG Spectrometer, and a POSS Doppler Radar,
647 Journal of Atmospheric and Oceanic Technology, 11, 874-887, 10.1175/1520-
648 0426(1994)011<0874:CORSDM>2.0.CO;2, 1994.

649 Steiner, M., Smith, J. A., and Uijlenhoet, R.: A Microphysical Interpretation of Radar
650 Reflectivity–Rain Rate Relationships, Journal of the Atmospheric Sciences, 61, 1114-1131,
651 10.1175/1520-0469(2004)061<1114:AMIORR>2.0.CO;2, 2004.

652 Testud, J., Oury, S., Black, R. A., Amayenc, P., and Dou, X.: The Concept of “Normalized”
653 Distribution to Describe Raindrop Spectra: A Tool for Cloud Physics and Cloud Remote

654 Sensing, Journal of Applied Meteorology, 40, 1118-1140, 10.1175/1520-
655 0450(2001)040<1118:TCOND>2.0.CO;2, 2001.

656 Thompson, E. J., Rutledge, S. A., Dolan, B., and Thurai, M.: Drop Size Distributions and Radar
657 Observations of Convective and Stratiform Rain over the Equatorial Indian and West
658 Pacific Oceans, Journal of the Atmospheric Sciences, 72, 4091-4125, 10.1175/JAS-D-14-
659 0206.1, 2015.

660 Tokay, A., and Short, D. A.: Evidence from Tropical Raindrop Spectra of the Origin of Rain
661 from Stratiform versus Convective Clouds, Journal of Applied Meteorology, 35, 355-371,
662 10.1175/1520-0450(1996)035<0355:Efrso>2.0.Co;2, 1996.

663 Tokay, A., Kruger, A., and Krajewski, W. F.: Comparison of Drop Size Distribution
664 Measurements by Impact and Optical Disdrometers, Journal of Applied Meteorology, 40,
665 2083-2097, 10.1175/1520-0450(2001)040<2083:CODSDM>2.0.CO;2, 2001.

666 Tokay, A., Bashor, P. G., Habib, E., and Kasparis, T.: Raindrop Size Distribution Measurements
667 in Tropical Cyclones, Monthly Weather Review, 136, 1669-1685,
668 10.1175/2007mwr2122.1, 2008.

669 Tokay, A., Petersen, W. A., Gatlin, P., and Wingo, M.: Comparison of Raindrop Size
670 Distribution Measurements by Collocated Disdrometers, Journal of Atmospheric and
671 Oceanic Technology, 30, 1672-1690, 10.1175/JTECH-D-12-00163.1, 2013.

672 Tu, J.-Y., and Chou, C.: Changes in precipitation frequency and intensity in the vicinity of
673 Taiwan: typhoon versus non-typhoon events, Environmental Research Letters, 8, 014023,
674 10.1088/1748-9326/8/1/014023, 2013.

675 Ulbrich, C. W., and Atlas, D.: Microphysics of Raindrop Size Spectra: Tropical Continental and
676 Maritime Storms, *Journal of Applied Meteorology and Climatology*, 46, 1777-1791,
677 10.1175/2007JAMC1649.1, 2007.

678 van Dijk, A. I. J. M., Bruijnzeel, L. A., and Rosewell, C. J.: Rainfall Intensity–Kinetic Energy
679 Relationships: A Critical Literature Appraisal, *Journal of Hydrology*, 261, 1-23,
680 10.1016/S0022-1694(02)00020-3, 2002.

681 Wen, L., Zhao, K., Chen, G., Wang, M., Zhou, B., Huang, H., Hu, D., Lee, W.-C., and Hu, H.:
682 Drop size distribution characteristics of seven typhoons in China, *J. Geophys. Res. Atmos.*,
683 123, 6529–6548, doi:10.1029/2017JD027950, 2018.

684 Wen, L., Zhao, K., Wang, M., and Zhang, G.: Seasonal Variations of Observed Raindrop Size
685 Distribution in East China, *Advances in Atmospheric Sciences*, 36, 346-362, 2019.

686 Wischmeier, W. H.: A Rainfall Erosion Index for a Universal Soil-Loss Equation¹, *Soil Science*
687 *Society of America Journal*, 23, 246-249, 10.2136/sssaj1959.03615995002300030027x,
688 1959.

689 Wu, Z., Zhang, Y., Zhang, L., Lei, H., Xie, Y., Wen, L., and Yang, J.: Characteristics of summer
690 season raindrop size distribution in three typical regions of western Pacific, *Journal of*
691 *Geophysical Research: Atmospheres*, 124, 4054-4073, 2019.

692 Zhang, Y., Liu, L., Bi, S., Wu, Z., Shen, P., Ao, Z., Chen, C., and Zhang, Y.: Analysis of dual-
693 polarimetric radar variables and quantitative precipitation estimators for landfall typhoons
694 and squall lines based on disdrometer data in southern China, *Atmosphere-Basel*, 10, 30,
695 2019.

696

697

698 **Table 1.** The JWD and rain gauge comparison results (n: number of rainy days, CC:
699 correlation coefficient, RMSE: root mean square error) for different wind speed
700 conditions (daily maximum wind speed: 0-8, 8-14, 14-18, > 18 m s⁻¹). Note: there
701 were no NTY rainy days with daily maximum wind speed > 14 m s⁻¹.

Wind speed (m s ⁻¹)	TY			NTY		
	n	CC	RMSE (mm)	n	CC	RMSE (mm)
0-8	21	0.989	6.305	113	0.956	3.853
8-14	27	0.99	5.153	18	0.942	3.482
14-18	8	0.953	18.112	-	-	-
>18	3	0.996	7.448	-	-	-

702

703

704

705

706

707

708

709

710

711 **Table 2.** Rainy minutes (N), mean, standard deviation (Std), Skewness and Kurtosis of seven
712 rainfall rate classes for typhoon (TY) and non-typhoon (NTY) rainy days of summer
713 seasons.

Rain rate class	Rain rate threshold (mm h ⁻¹)	Typhoon (TY)					non-typhoon (NTY)				
		No. of samples	Mean (mm h ⁻¹)	Standard deviation (mm h ⁻¹)	Skewness	Kurtosis	No. of samples	Mean (mm h ⁻¹)	Standard deviation (mm h ⁻¹)	Skewness	Kurtosis
C1	$0.1 \leq R < 1$	9317	0.43	0.26	0.55	2.1	10661	0.4	0.25	0.71	2.34
C2	$1 \leq R < 2$	3274	1.44	0.29	0.24	1.84	3193	1.43	0.29	0.29	1.88
C3	$2 \leq R < 5$	4747	3.29	0.85	0.31	1.92	3404	3.17	0.83	0.46	2.1
C4	$5 \leq R < 10$	2799	7	1.4	0.43	2.04	1404	6.98	1.42	0.43	2.01
C5	$10 \leq R < 30$	2313	16.44	5.24	0.77	2.59	1234	17.46	5.6	0.5	2.08
C6	$30 \leq R < 50$	393	38.31	5.73	0.37	1.92	320	37.88	5.67	0.45	2.01
C7	$R > 50$	231	67.15	14.91	1.16	3.97	152	65.86	14.94	1.51	5.18
total		23074	4.88	9.38	4.59	31.51	20368	3.59	8.38	5.2	38.9

714

715

716

717 **Table 3.** Statistical parameters [correlation coefficient: R^2 , Root mean square error (RMSE),
718 normalized RMSE] for typhoon (TY) and non-typhoon (NTY) rainy days. Note: Units for
719 RMSE are $J m^{-2} h^{-1}$ for KE_{time-R} relations and $J m^{-2} mm^{-1}$ for KE_{mm-R} and KE_{mm-D_m}
720 relations.

Weather condition	Statistical parameter	KE_{time-R}		KE_{mm-R}			KE_{mm-D_m}
		Linear	Power	Power	Exp	Log	Second order polynomial
TY	R^2	0.986	0.994	0.694	0.68	0.68	0.992
	RMSE	37.488	24.785	3.973	10.227	4.047	12.396
	NRMSE	0.306	0.202	0.032	0.083	0.033	2.514
NTY	R^2	0.984	0.99	0.646	0.639	0.639	0.988
	RMSE	38.012	30.745	4.599	11.017	4.636	12.93
	NRMSE	0.322	0.26	0.039	0.093	0.039	2.803

721

722

723

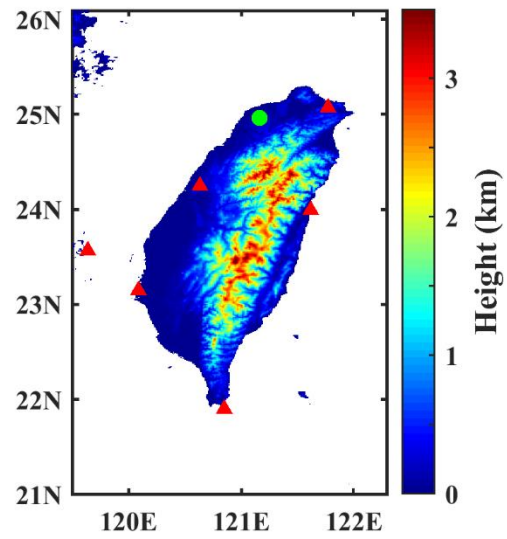
724

725

726

727

Figures



728

729 **Figure 1.** Map of Taiwan with disdrometer (green color circle) and radars (red color triangles)

730 sites.

731

732

733

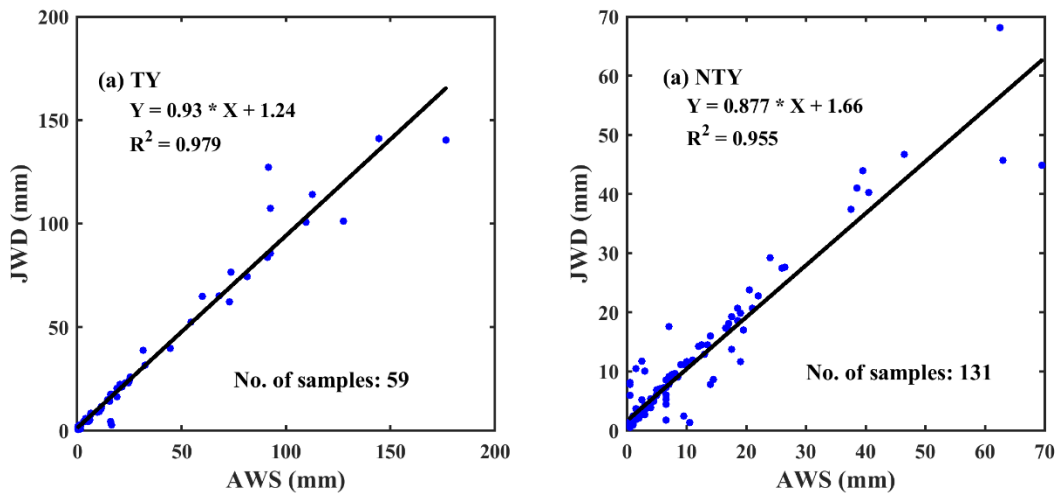
734

735

736

737

738



739

740 **Figure 2.** The JWD and rain gauge daily accumulations scatter plot for (a) typhoon (TY) and (b)

741 non-typhoon (NTY) rainfall.

742

743

744

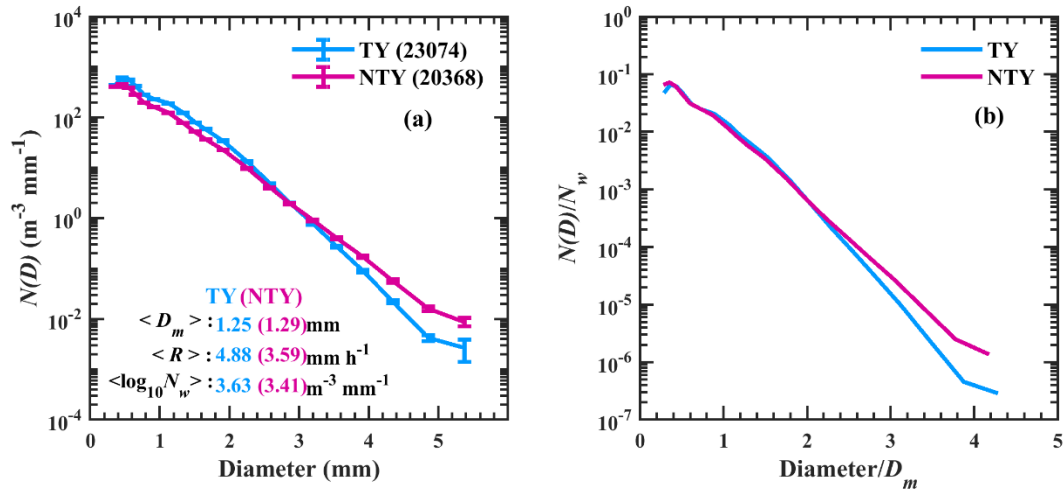
745

746

747

748

749



750

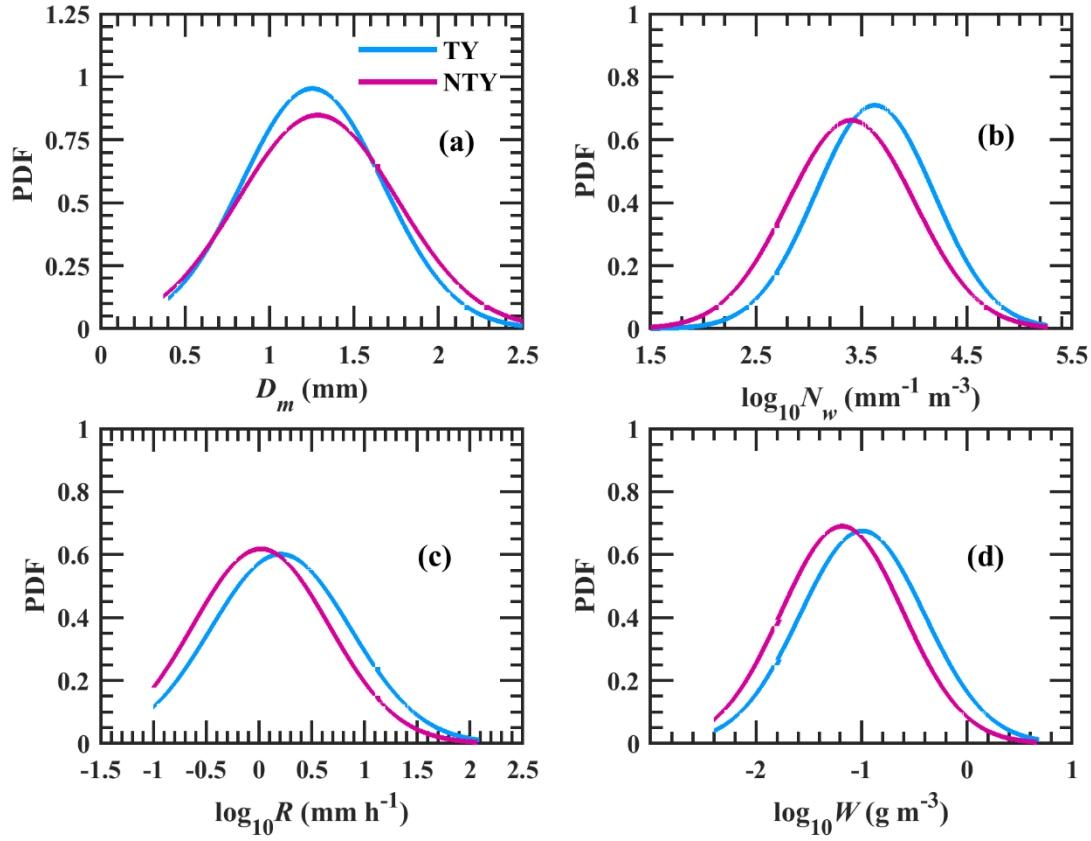
751 **Figure 3.** (a) Distributions of mean concentration [$N(D)$, in $\text{mm}^{-1} \text{m}^{-3}$] with raindrop diameter
 752 for typhoon (TY) and non-typhoon (NTY) rainfall and their (b) normalized spectra.

753

754

755

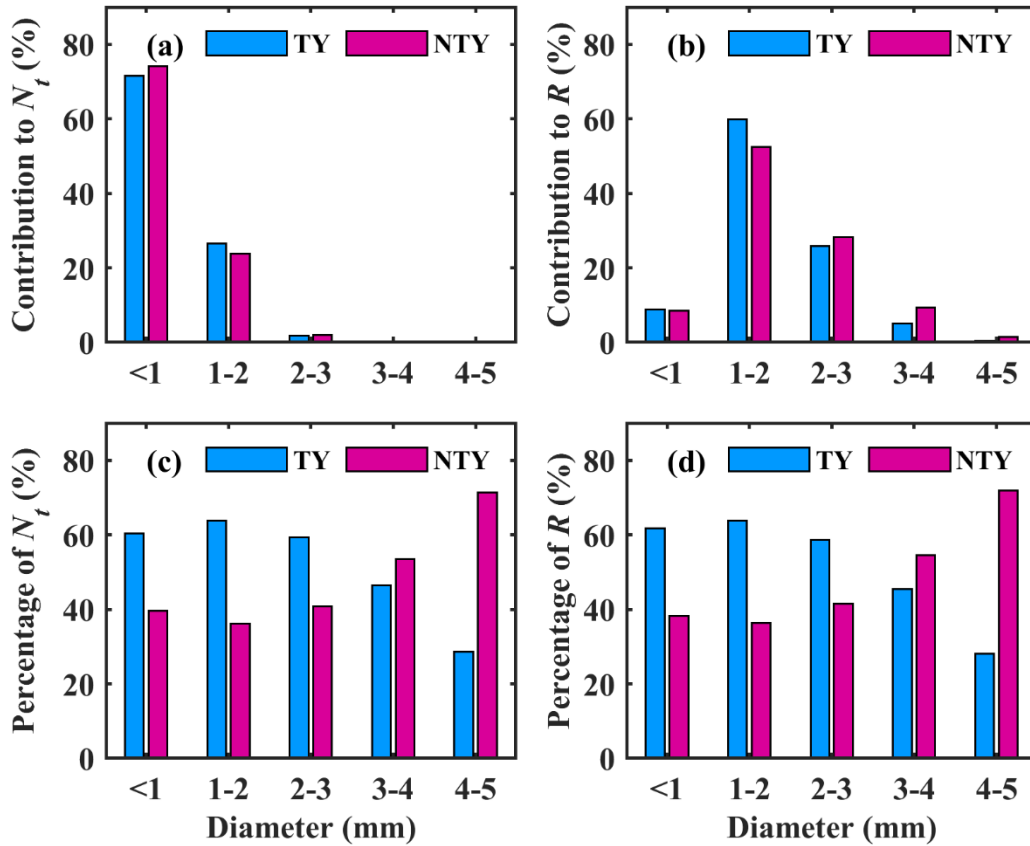
756



757

758 **Figure 4.** The probability distribution functions (PDF) of (a) mass-weighted mean diameter, D_m
 759 (mm), (b) $\log_{10} N_w$ (N_w is the normalized intercept parameter in $\text{mm}^{-1} \text{m}^{-3}$), (c) $\log_{10} R$ (R
 760 is rainfall rate in mm h^{-1}), and (d) $\log_{10} W$ (W is the liquid water content in g m^{-3}) for
 761 typhoon (TY) and non-typhoon (NTY) rainfall.

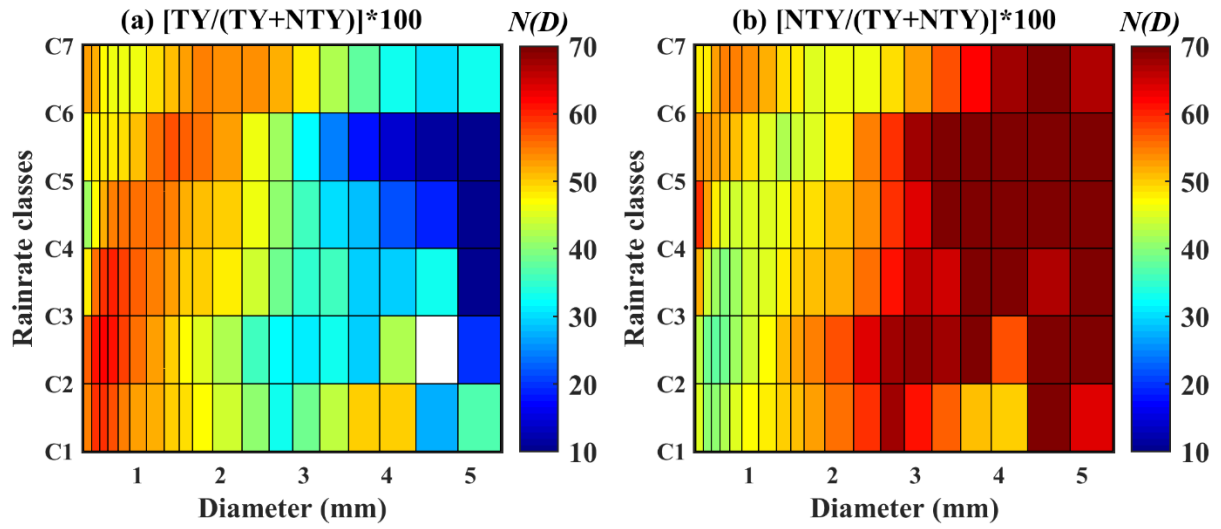
762



763

764 **Figure 5.** Contribution of drop diameter classes (Diameter < 1 mm, 1–2 mm, 2–3 mm, 3–4 mm,
 765 and 4–5 mm) to (a) total number concentration N_t (m^{-3}) and (b) rainfall rate R (mm h^{-1})
 766 in typhoon (TY) and non-typhoon (NTY) rainfall. Occurrence percentage of (c) total
 767 number concentration N_t (m^{-3}) and (d) rainfall rate R (mm h^{-1}) in each diameter class for
 768 typhoon (TY) and non-typhoon (NTY) rainfall.

769



770

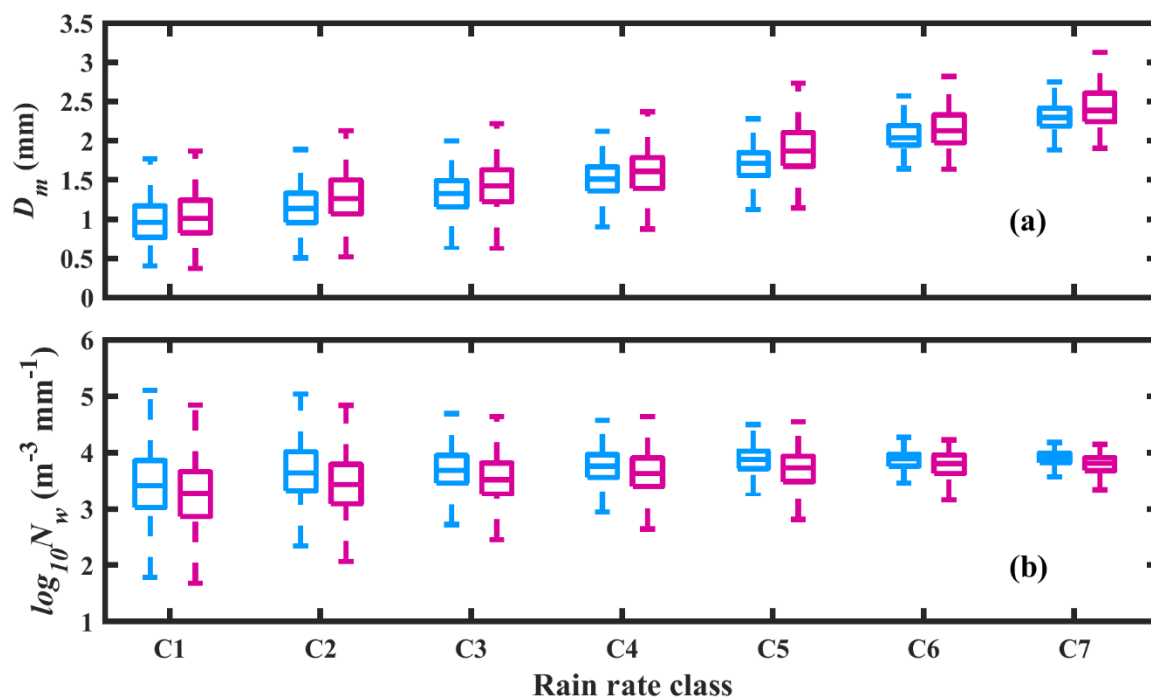
771 **Figure 6** Percentage contribution of $N(D)$ ($\text{mm}^{-1} \text{m}^{-3}$) in different rainfall rate classes for
 772 typhoon (TY) and non-typhoon (NTY) rainfall.

773

774

775

776



777

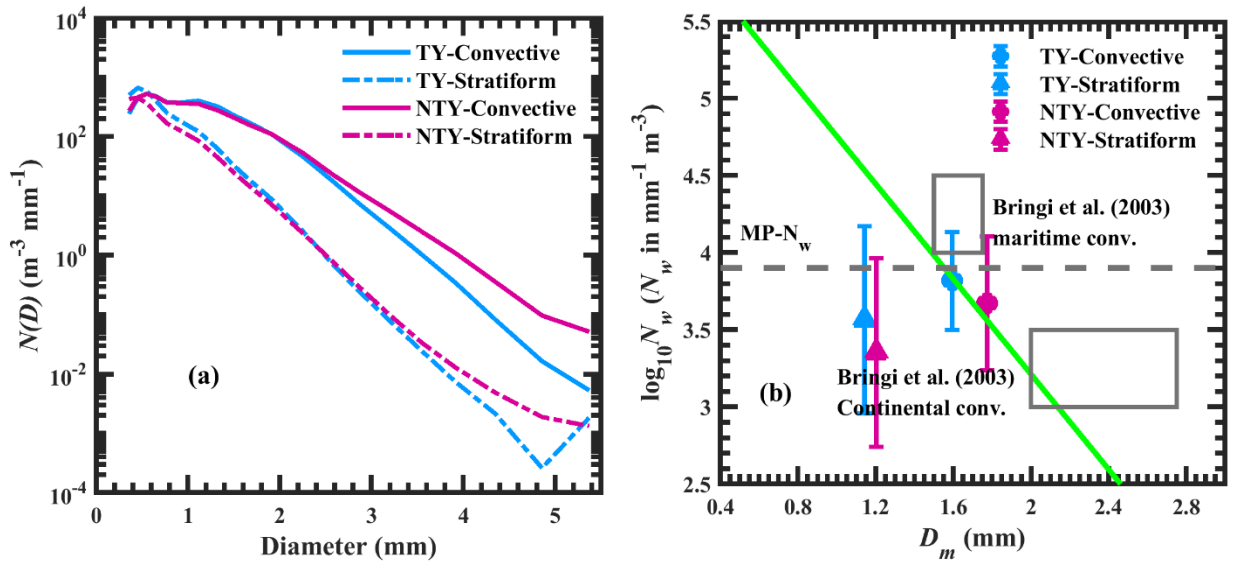
778 **Figure 7.** Box plot of (a) D_m (mm) and (b) $\log_{10} N_w$ ($\text{mm}^{-1} \text{m}^{-3}$) in seven rainfall rate classes for
 779 typhoon (TY) (sky blue color) and non-typhoon (NTY) (dark magenta) rainfall. The
 780 center line of the box indicates the median, and the bottom and top lines of the box
 781 indicate the 25th and 75th percentiles, respectively. The bottom and top of the dashed
 782 vertical lines indicate the 5th and 95th percentiles, respectively.

783

784

785

786



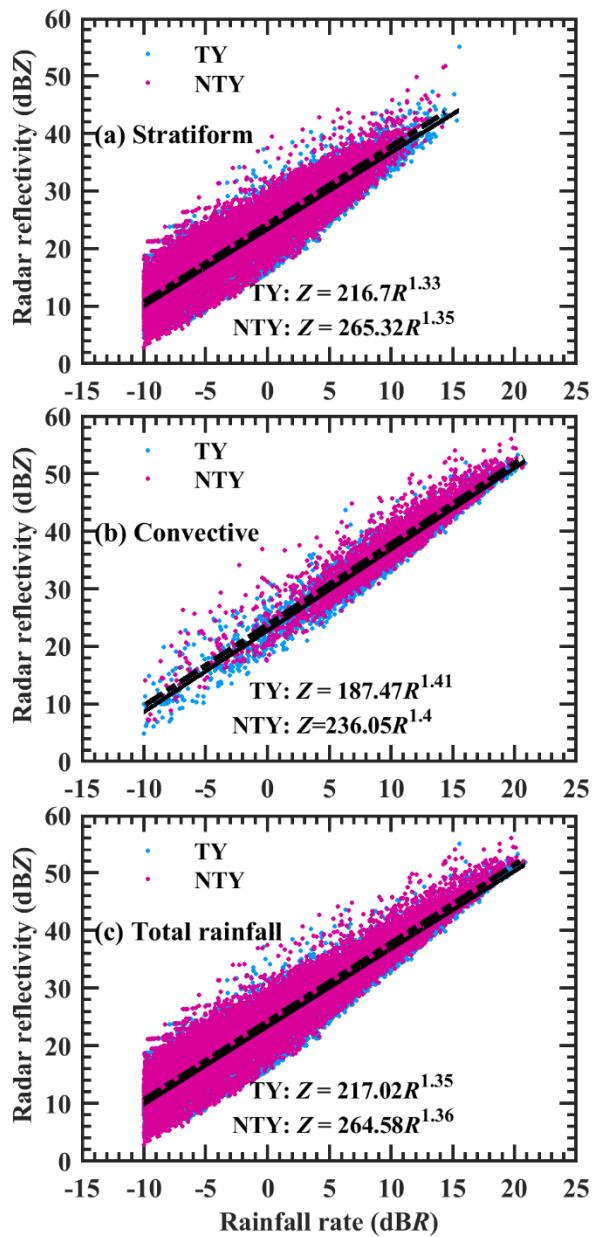
787

788 **Figure 8.** (a) Distribution of $N(D)$ ($\text{m}^{-3} \text{mm}^{-1}$) with raindrop diameter in stratiform and
 789 convective precipitation for typhoon (TY) and non-typhoon (NTY) rainfall. (b)
 790 Variations of $\log_{10} N_w$ (where N_w is the normalized intercept parameter in $\text{mm}^{-1} \text{m}^{-3}$) with
 791 D_m (mass-weighted mean diameter in mm) in stratiform and convective regimes for
 792 typhoon (TY) and non-typhoon (NTY) rainfall. The horizontal gray dashed line is the
 793 Marshall-Palmer value of $\log_{10} N_w$ (3.9) for exponential shape. The green dash dotted line
 794 is the stratiform and convective separation line of Bringi et al. (2003).

795

796

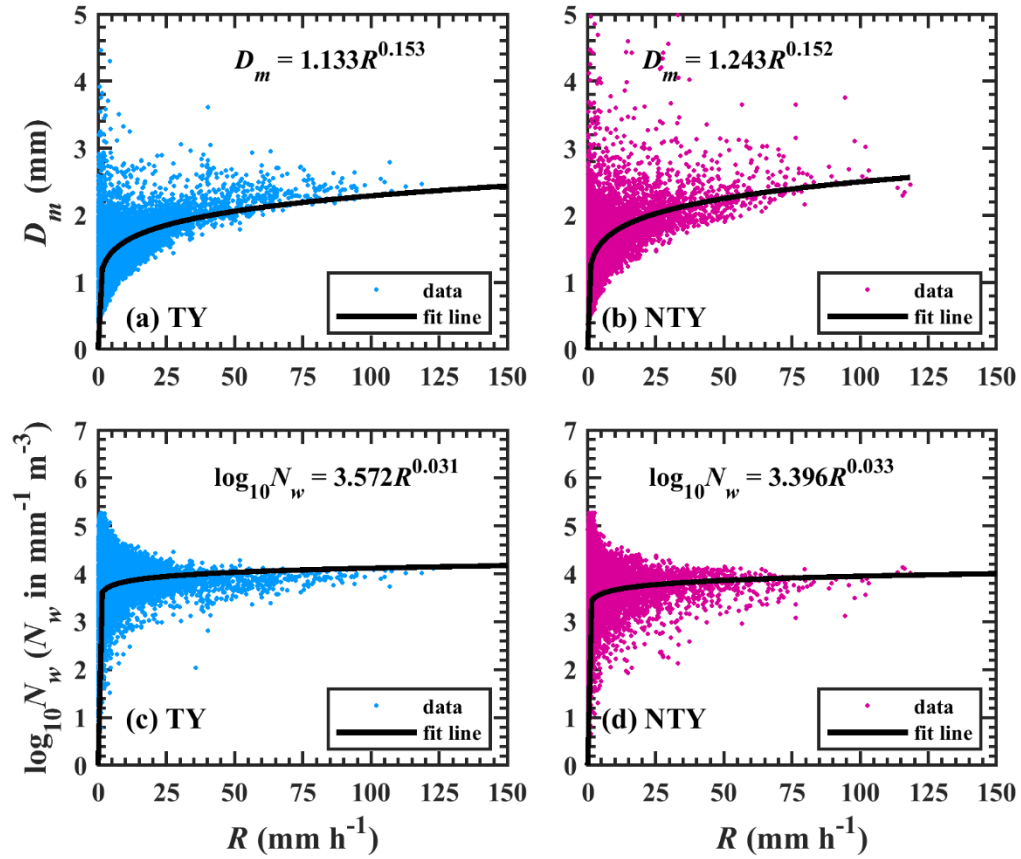
797



798

799 **Figure 09.** Scatter plots of radar reflectivity (Z , dBZ) and rainfall rate in logarithmic scale

800 $(10 \cdot \log_{10} R, \text{dBR}, R \text{ in } \text{mm h}^{-1})$ for typhoon (TY) and non-typhoon (NTY) rainfall.



801

802 **Figure 10.** Distributions of D_m (mm) and $\log_{10} N_w$ (N_w in $\text{mm}^{-1} \text{m}^{-3}$) with rainfall rate (R , mm

803 h^{-1}) for typhoon (TY) and non-typhoon (NTY) rainfall.

804 .

805

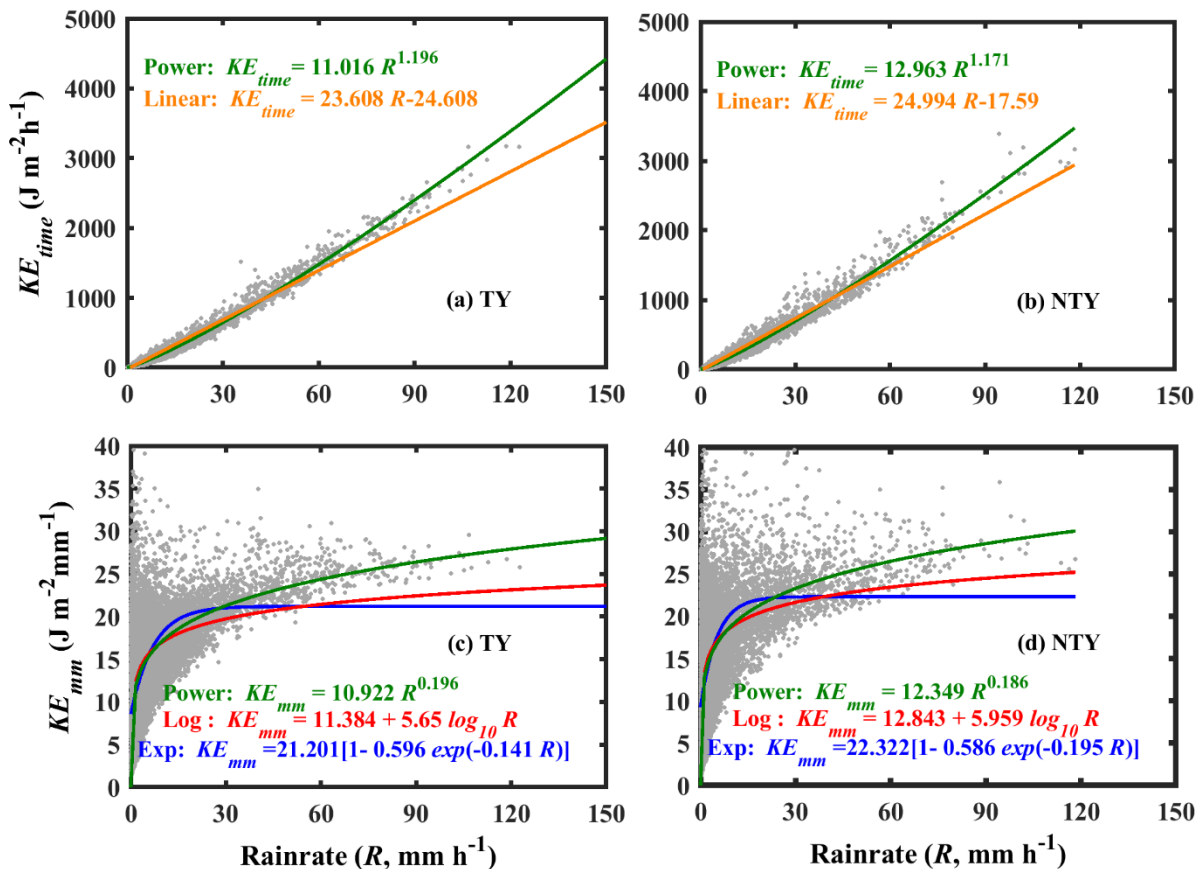
806

807

808

809

810



811

812 **Figure 11.** Scatter plots of rainfall kinetic energy (KE) [time-specific KE , KE_{time} ; volume-

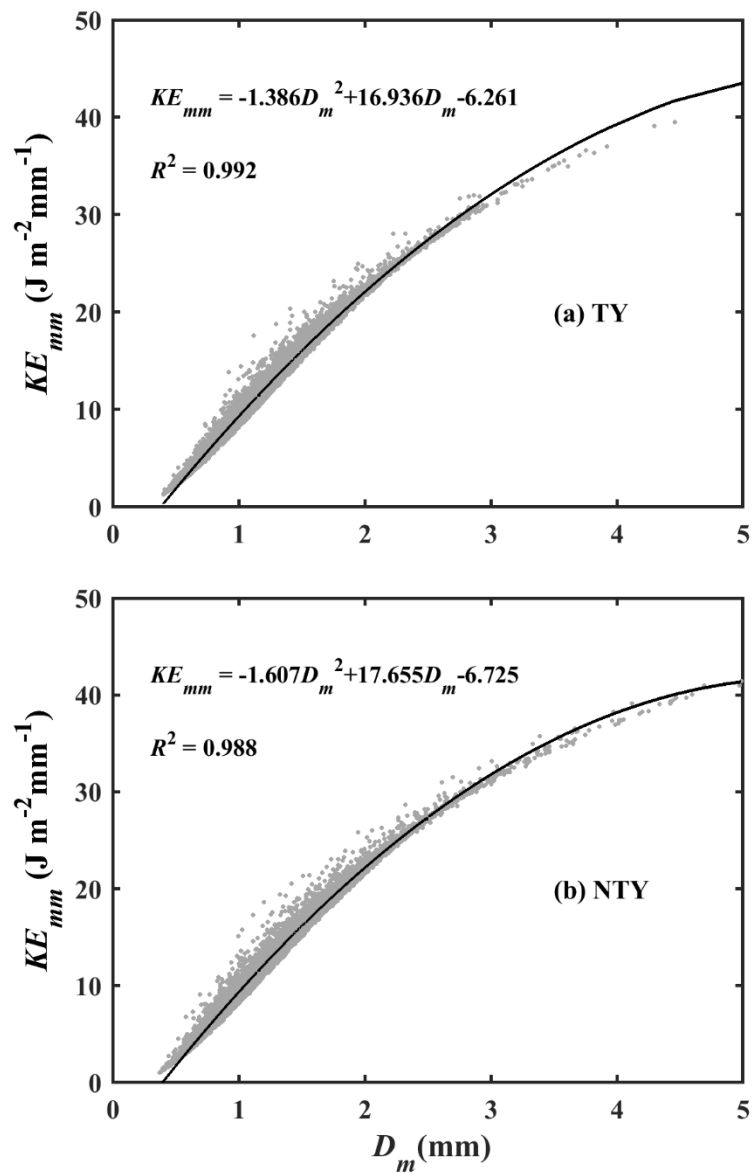
813 specific KE , KE_{mm}] with rainfall rate (R , mm h^{-1}) for typhoon (TY) and non-typhoon

814 (NTY) rainfall.

815

816

817



819

820 **Figure 12.** Scatter plots of volume-specific KE (KE_{mm} in $\text{J m}^{-2} \text{mm}^{-1}$] with D_m (mm) for typhoon

821 (TY) and non-typhoon (NTY) rainfall.

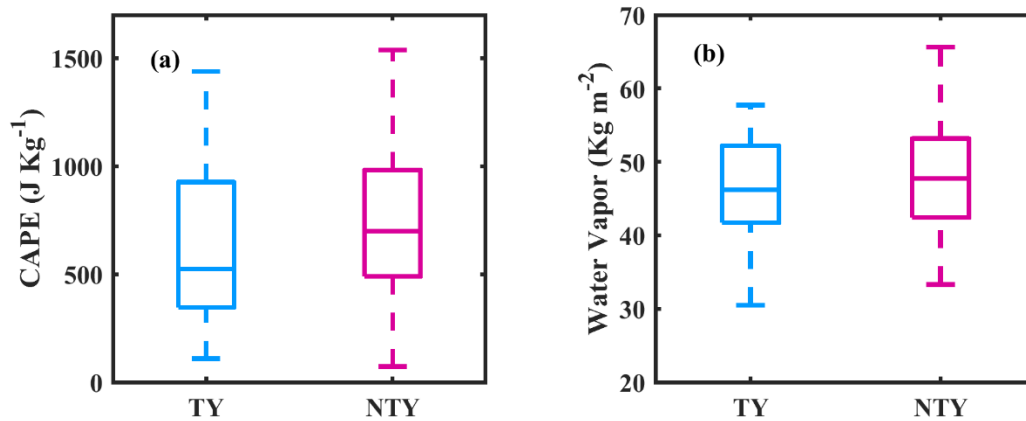
822

823

824

825

826



827

828 **Figure 13.** Variations in (a) convective available potential energy (CAPE, J Kg^{-1}) and (b)
829 vertical integral of water vapor (kg m^{-2}) for typhoon (TY) and non-typhoon (NTY)
830 rainfall. The center line of the box indicates the median, and the bottom and top lines of
831 the box indicate the 25th and 75th percentiles, respectively. The bottom and top of the
832 dashed vertical lines indicate the 5th and 95th percentiles, respectively

833

834

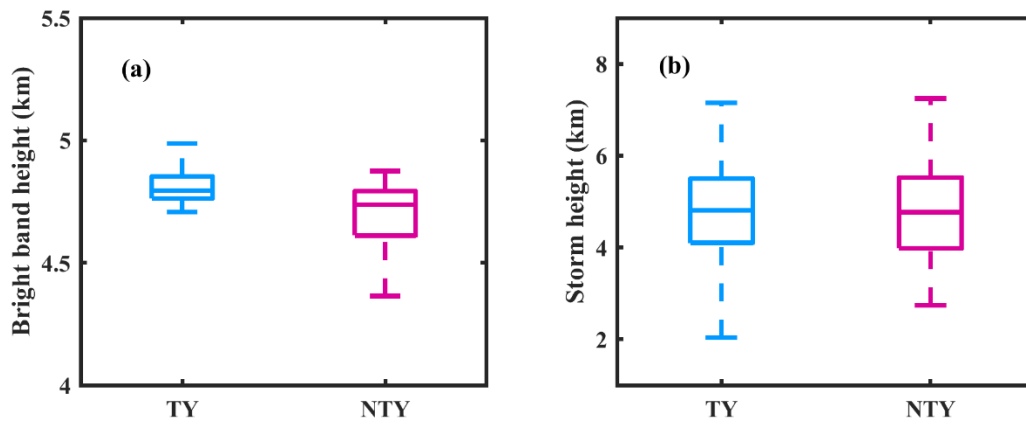
835

836

837

838

839



840

841 **Figure 14.** (a) Bright band (BB) and (b) storm heights box plots for typhoon (TY) and non-
842 typhoon (NTY) rainfall.

843

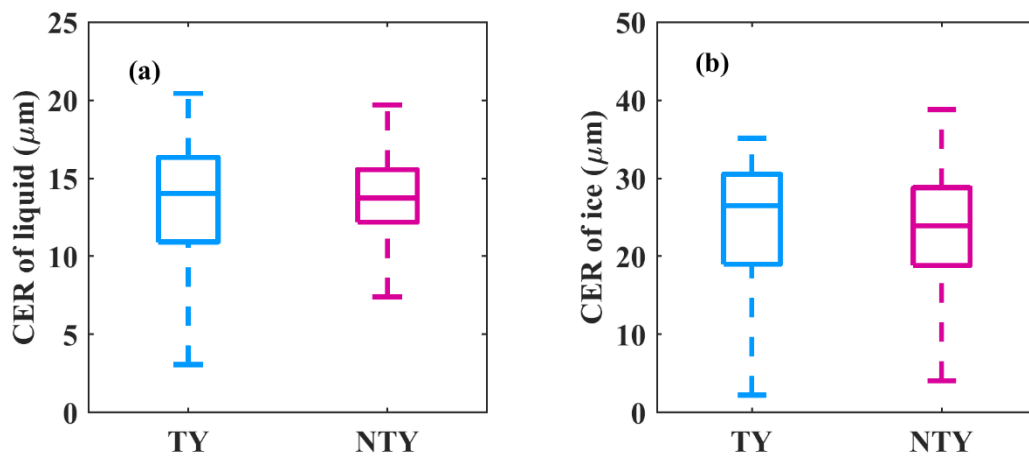
844

845

846

847

848



849

850 **Figure 15.** (a) Liquid, (b) ice particles cloud effective radii (CER, μm) values for typhoon (TY)

851 and non-typhoon (NTY) rainfall.

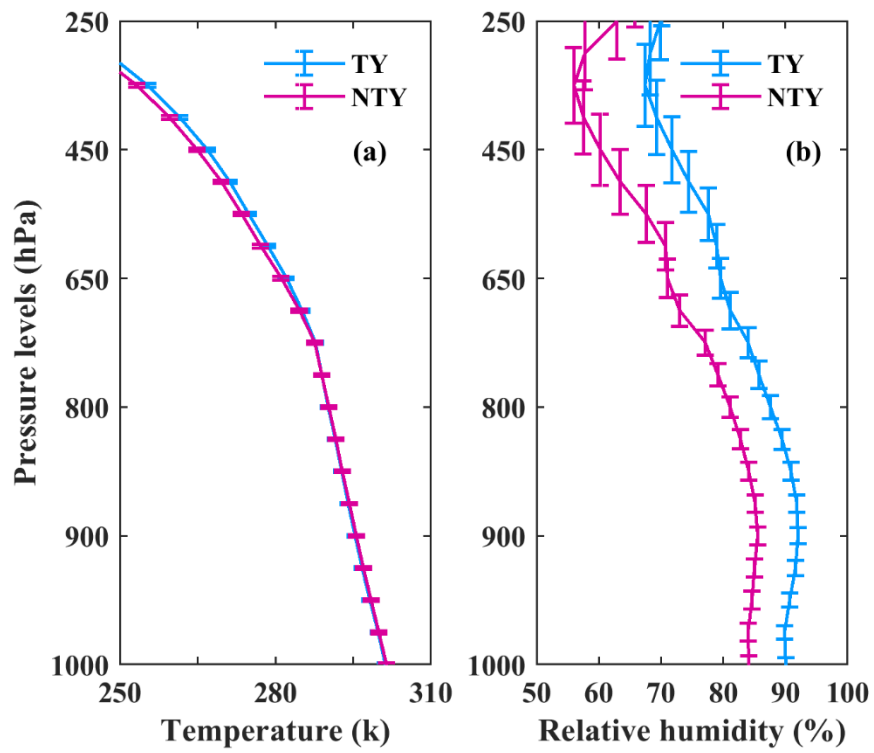
852

853

854

855

856



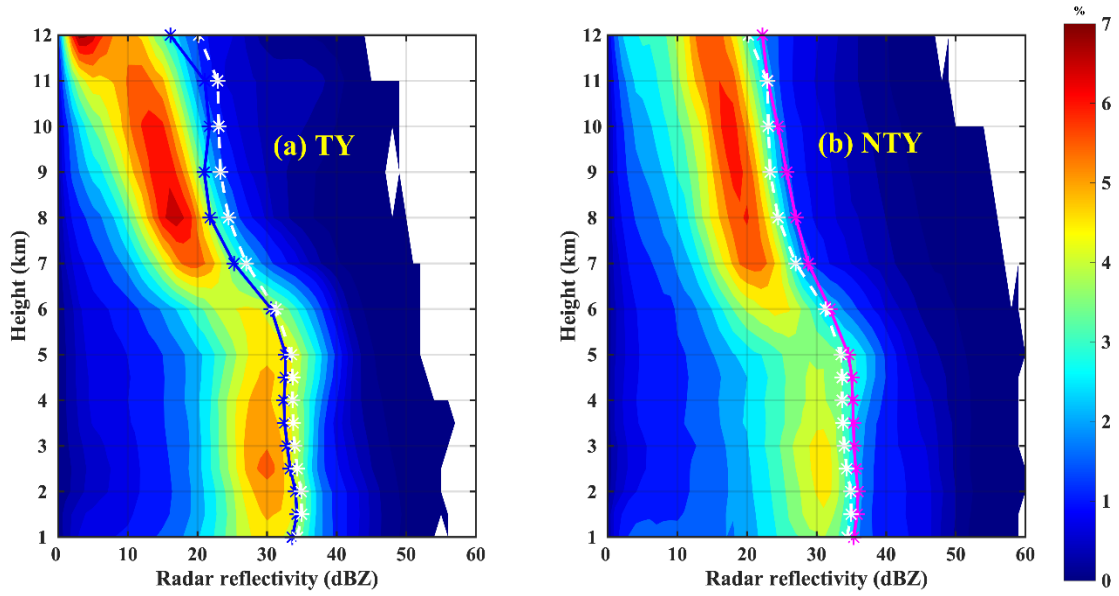
857

858 **Figure 16.** (a) Mean air temperature ($^{\circ}\text{C}$) and (b) relative humidity (%) profiles for typhoon (TY)
 859 and non-typhoon (NTY) rainfall.

860

861

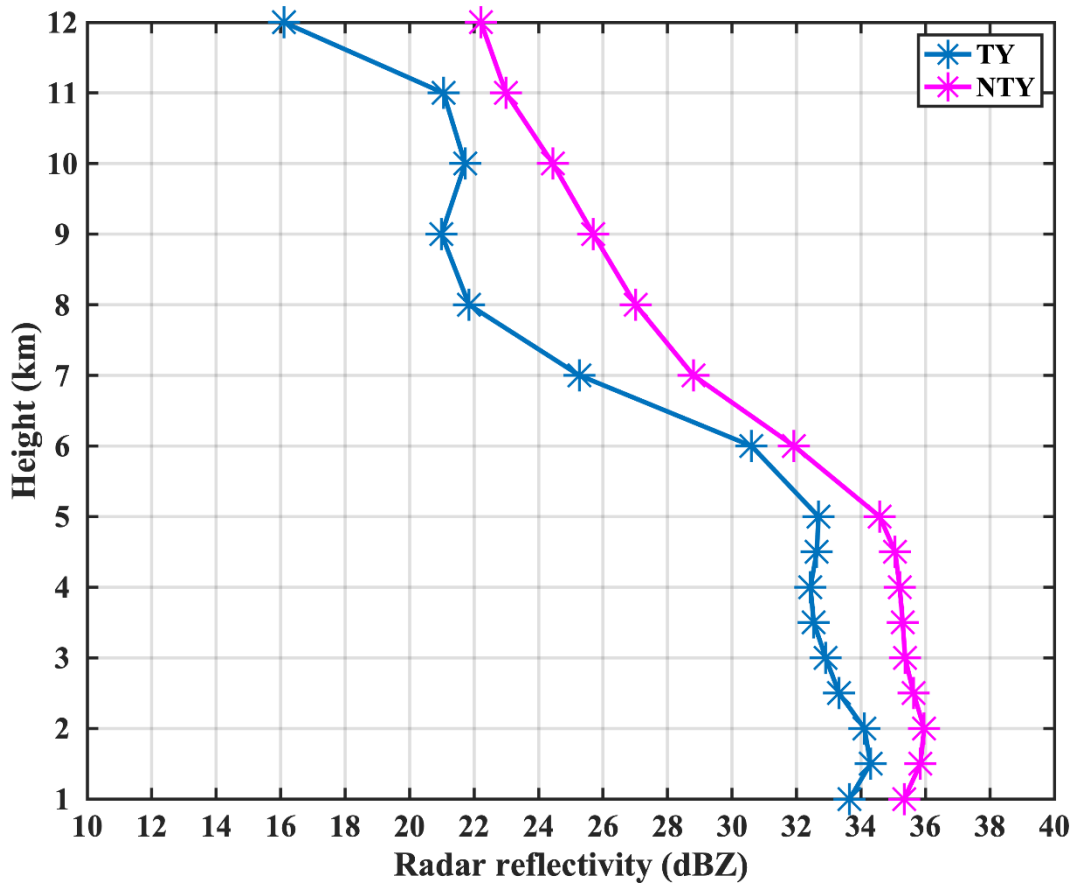
862



863

864 **Figure 17.** Radar reflectivity contoured frequency-by-altitude diagram (CFAD) from six ground-
 865 based radars for (a) typhoon (TY) and (b) non-typhoon (NTY) rainfall.

866



867

868 **Figure 18.** Mean radar reflectivity profiles of typhoon (TY) and non-typhoon (NTY) rainfall.

869

870